Optical Transmission Systems
For
Cable Television Applications

by

D'Arcy John Davidson
B.Eng., University of Victoria, 1990

A Thesis Submitted in Partial Fulfillment of the
Requirements for the Degree of

MASTER OF APPLIED SCIENCE

in the Department of Electrical and Computer Engineering

We accept this thesis as conforming to the required standard

[redacted]

Dr. R. Vahldieck, Supervisor (Dept. of Elec. & Comp. Eng.)

[redacted]

Dr. J. Bornemann, Dept. Member (Dept. of Elec. & Comp. Eng.)

[redacted]

Dr. G. McLean, Outside Member (Dept. of Mech. Eng.)

[redacted]

Dr. C. Bradley, External Examiner (Dept. of Mech. Eng.)

ABSTRACT

This thesis examines the use of fibre optic systems for the transmission of cable television signals. The low loss and high noise immunity of fibre optic systems make this technology a desirable alternative to the coaxial distribution systems presently in use, where many repeaters are necessary to carry the signal from head-end to subscriber. These repeaters both distort the signal and reduce the reliability of the transmission system. To be cost effective, fibre optic systems must be capable of transmitting the existing signal modulation formats. State-of-the-art optical transmitters can only transmit a limited number of channels due to noise and linearity constraints. This thesis theoretically and experimentally evaluates a new linearization scheme for externally modulated optical systems which increases the channel capacity by improving the linearity and reducing the noise of the optical transmitter. This scheme is capable of transmitting 100 channels using existing modulation formats and frequency allocations.

Examiners:

[redacted]

Dr. R. Vahldieck, Supervisor (Dept. of Elec. & Comp. Eng.)

[redacted]

Dr. J. Bornemann, Dept. Member (Dept. of Elec. & Comp. Eng.)

[redacted]

Dr. G. McLean, Outside Member (Dept. of Mech. Eng.)

[redacted]

Dr. C. Bradley, External Examiner (Dept. of Mech. Eng.)

TABLE OF CONTENTS

TABLE OF CONTENTS (Continued)

Page

LIST OF FIGURES

Page

LIST OF FIGURES (Continued)

Page

LIST OF TABLES

Page

ACKNOWLEDGMENTS

I would like to thank Dr. Vahldieck for his guidance and suggestions. Special thanks go to my wife Amanda, without whose encouragement and support I would never have finished. I would like to also thank Canadian Cable Labs, Rogers Communications Inc., and NSERC for their financial assistance in this project.

1. INTRODUCTION

The migration of fibre optic transmission systems from the laboratory to the commercial market has had dramatic effects on present-day communications technology. Fibre optic systems have improved the quality and quantity of voice and data transmission around the world. The majority of optical communications systems in use today employ digital technology to transmit information, as this provides high quality transmission that is easily switched to and from various subscribers. In addition, the ever increasing quantity of computer traffic is in a digital format. Digital optical transmission systems are relatively easy to design and provide reliable, high speed data transmission.

Analog optical transmission systems have not seen the same level of attention as digital systems because the applications for analog transmission are more specialized. For example, analog signal formats are desirable in today's cable television (CATV) applications because of the direct compatability with analog television sets and the low losses of fibre. Analog systems are also useful for carrying microwave signals to and from radio transceivers over long distances. The design of analog optical transmission systems presents many challenges due to the non-linear and noisy nature of optical transmitters.

This thesis focuses on the use of the fibre optic medium for transmission of CATV signals. Although there is little question that digital television will one day become standard, there are still many obstacles to overcome before this becomes reality. In the interim, there is a need for wideband low-noise linear

optical systems that are compatible with existing CATV transmission equipment and television receivers.

Fibre-optic transmission of CATV signals promises many advantages over coaxial-based systems mainly due to the high bandwidth of optical carriers and low losses of fibre. However, the vestigial-sideband amplitude modulated (VSB-AM) signal format presently used in CATV systems requires a carrier-to-noise ratio (CNR) near 50 dB for good picture quality. In addition, the many distortion products generated by system non-linearities must have a cumulative power that is more than 60 dB below the carrier level. Meeting these requirements using amplitude modulated lightwave systems has proven to be feasible but difficult in view of the fact that a sensitive compromise exists between CNR and linearity. This tradeoff can be eased by employing various linearization schemes. In order for these schemes to be effective, however, optical sources with sufficient power and low noise must be employed to satisfy signal-to-noise ratio (SNR) and power budget specifications.

In this thesis, we propose a linearization option for externally modulated optical transmitters which is suitable for the distribution of 100 or more channels. For 40-60 channels, state-of-the-art commercially available distributed feedback lasers can satisfy the strict composite second order (CSO), composite triple beat (CTB), and SNR requirements demanded by CATV operators. However, these systems typically have an optical power budget of only 5 dB, which leaves little headroom for signal distribution. The scheme presented in this thesis essentially pre-distorts the electrical signal using one electro-optic modulator (EOM) of a matched pair. This type of

linearization (referred to as Quasi-Feedforward) has been applied in the past to linearize light emitting diodes (LEDs) with limited success [1]. This scheme is difficult to implement with semiconductor devices due to the large statistical variation in device characteristics and due to changes in these characteristics over time. The use of EOMs solves this problem and also provides a means of partially cancelling the relative intensity noise (RIN) introduced by the optical source.

Quasi-Feedforward is examined theoretically and experimentally for use with CW optical sources and conventional Mach-Zehnder type modulators, as well as with linearized modulators which are now emerging on the market. We show theoretically that 100 channels can be carried with a 52 dB carrier-to-noise-ratio using a CW laser with a RIN of -130 dB/Hz. The power budget of this scheme is limited only by the power of the CW source and fiber non-linearities.

2. THE NTSC TELEVISION SIGNAL

2.1 The Unmodulated Video Signal

The baseband signal format used for the transmission of video in cable television networks is identical to that used in off-air broadcasts, and is referred to as the NTSC standard. This standard was developed in 1940 by the National Television Standards Committee and came into widespread use shortly thereafter. The following description of the standard focuses only on those parameters important to the development of this thesis, and is in no way comprehensive. The interested reader is encouraged to reference some of the many books available on the subject [6, 36-39].

Figure 2.1 shows a time domain snapshot of a NTSC video signal. The signal shown corresponds to a single horizontal line of video, and if viewed on a TV it would be a line with increasing intensity from black to white. The standard video level is 1 $V_{p\text{-}p}$ from peak white to the synchronization pulse tips, when terminated in a 75 Ω load. An alternative signal scale developed by the Institute of Radio Engineers is appropriately termed the IRE scale [38]. The amplitude of the video signal using this measurement is 140 IRE including the sync pulse as shown in Figure 2.1. The line period is 1/15.75 KHz, or 63.5 μs, where 15.75 KHz is the line scanning frequency. The video signal is divided into two parts, luminance (brightness) and chrominance (color). The luminance signal occupies the full video bandwidth from 0 to 4.2 MHz. The chrominance signal itself comprises two parts, both of which are modulated on a 3.58 MHz color subcarrier. The color subcarrier directly interferes with the luminance information and vise-versa. This was a compromise that was made when color television became commonplace in

order to maintain compatibility with existing black and white technology. The NTSC standard has a 525 line screen, of which many lines cannot be seen due to vertical synchronization and retrace time. The entire screen is refreshed every 1/30th of a second. To reduce flicker, the lines are interlaced such that all odd and even lines are updated alternately at a rate of 1/60th of a second each. The combination of chrominance and luminance information, as well as horizontal and vertical synchronizing information, comprises a composite video signal. Peak white corresponds to 100 IRE and peak black corresponds to 0 IRE.

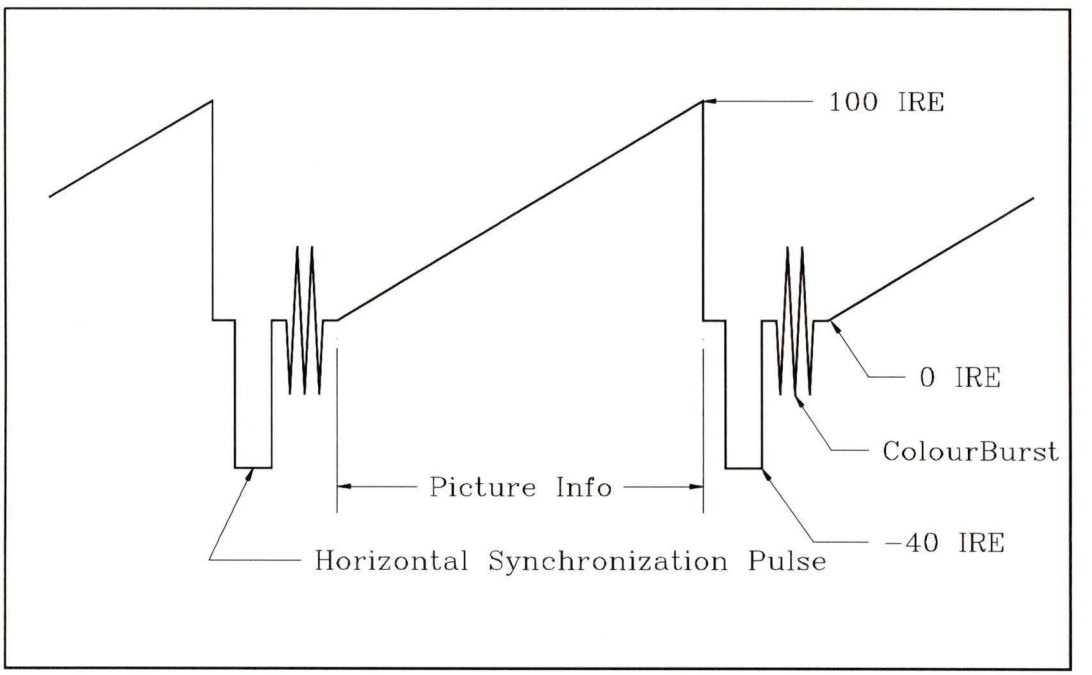

Figure 2.1 - The NTSC video signal

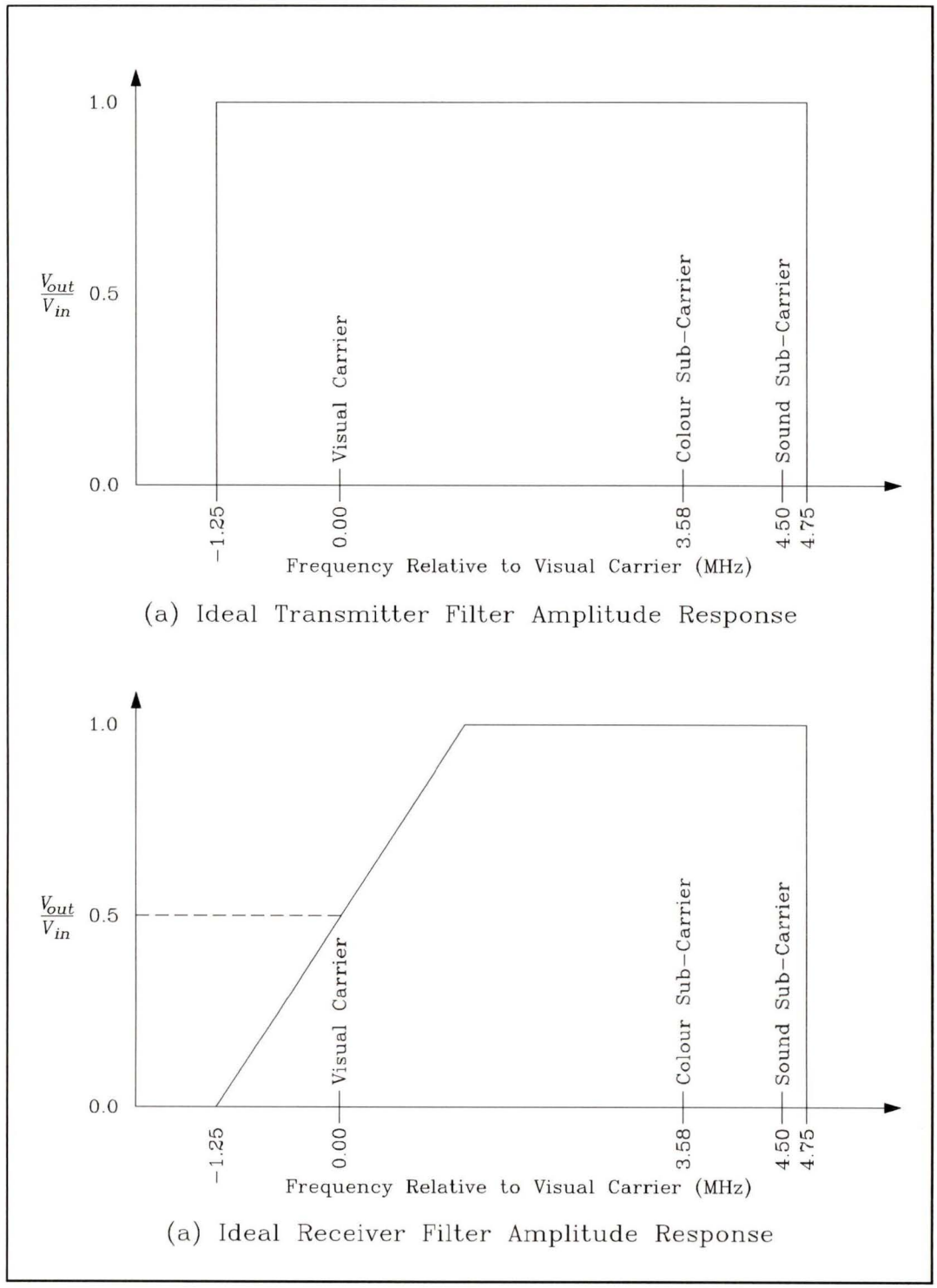

Figure 2.2 - Filter used for Tx and Rx of VSB-AM video signals

2.2 The Modulated Video Signal

The baseband video signal is modulated in a VSB-AM format for both air-wave and cable distribution. This format offers excellent bandwidth efficiency compared to frequency modulated schemes, and allows many channels to be broadcast or distributed in a minimum bandwidth.

To create a VSB-AM signal, the composite video signal is first amplitude modulated at a modulation factor of 0.778. The modulation is in a negative sense in that the peak carrier level corresponds to the synchronization tips. This is done so that the noise added during transmission will be most prominent in dark areas of the picture, and thus less noticeable to the viewer. This signal is then (ideally) passed through a brickwall bandpass filter (Figure 2.2a) with lower cutoff frequency $(f_c - 1.25)$ MHz and upper cutoff frequency $(f_c + 4.75)$ MHz, where f_c is the visual carrier frequency. If this signal was envelope detected at this point, the message signal amplitude would be attenuated by 6dB at frequencies greater than 1.25 MHz, which would result in significant signal distortion.

The television receiver compensates for this by passing the broadcast signal through another filter as shown in Figure 2.2b. This filter has a Nyquist response and reduces the carrier amplitude by a factor of two. The result of this filter followed by an envelope detector is a demodulated signal with a flat frequency response.

One VSB-AM signal occupies a bandwidth of 6 MHz. The video signal has a maximum bandwidth of 4.2 MHz, and there is a 1.25 MHz lower sideband. This consumes 5.45 MHz. The remainder of the bandwidth is allocated for

the aural (sound) carrier, which is frequency modulated on a carrier 4.5 MHz above the visual carrier. In broadcast systems, the aural carrier level is typically 2-3 dB below the visual carrier level. In CATV applications, however, the aural carrier level should be no less than 10 dB and no more than 20 dB below the visual carrier level. This difference is accountable to the fact that cable systems transmit adjacent channels, and it is very difficult to sufficiently filter the lower sideband to prevent interference with the lower adjacent channel.

2.3 Video Signal-to-Noise Ratio

The video signal-to-noise ratio gives a measure of picture quality. The average signal-to-noise ratio (SNR) in subscriber CATV systems is between 43 and 47 dB, where 47 dB is the threshold of human perception. It is fruitless to design a system with a better signal-to-noise ratio, except to provide some headroom for changes in system parameters due to component aging, and to prevent further degradation to signals that have marginal quality at the source. Main distribution trunks often have better SNR's to allow for further degradation between distribution hubs and the subscriber.

The relationship between video signal-to-noise ratio and carrier-to-noise ratio (CNR) is important for determining the effect of channel noise on received signal quality. There are two standards for measuring video signal-to-noise ratios, namely CCIR recommendation 567 and NTC 7 [7]. These two standards both specify a weighted and unweighted measurement. The unweighted measurement measures the noise power across a specified bandwidth. The weighted approach filters the noise as a function of

frequency, because high frequency noise is less perceptible to the eye than low frequency noise. This approach thus gives a higher SNR value. Both standards take the video signal level to be 100 IRE (peak white) or 714 mV.

The CCIR standard calculates the unweighted noise in a 5 MHz bandwidth, whereas the NTC standard calculates it in a 4.2 MHz bandwidth. The weighting characteristics are different for each as well. Assuming the noise power density is constant with frequency, the CCIR weighted SNR is approximately 7.2 dB better than the unweigted SNR, and the NTC weighted SNR is about 5.7 dB better than the unweighted SNR.

Consider the AM signal given by :

$$s(t) = [1 + 1.55 \cdot m(t)] \cdot \cos(2\pi \cdot f_c \cdot t) \tag{2.1}$$

where $m(t)$ is an inverted video signal with the synchronization tips at +0.5 V and peak white at -0.5 V, and f_c is the carrier frequency. The carrier-to-noise ratio of this signal is:

$$CNR = \frac{\text{Carrier Power}}{\text{Noise Power}} = \frac{(1 + 1.55 \cdot 0.5)^2}{2 \cdot N_o \cdot B} = \frac{1.58}{N_o \cdot B} \tag{2.2}$$

where N_o is the noise spectral density, and B is the measurement bandwidth, taken to be 4.2 MHz in the discussion that follows. The factor of 0.5 in the numerator of equation 2.2 is due to the fact that the carrier power is taken to be the average power during the synchronization pulse. The amplitude of the synchronization pulse is not affected by the reduction in lower sideband width, because most of its frequency components are less than 1.25 MHz.

The received SNR ratio of a VSB-AM system works out to be exactly one-half of that for an AM system. The VSB filter located in the receiver reduces the signal power by four compared to an AM system, and reduces the noise only by a factor of two, due to the lower bandwidth. Thus the signal-to-noise ratio of the demodulated signal given by equation (2.2) is [4] :

$$SNR = \frac{(1.55)^2 \cdot (0.714)^2}{4 \cdot N_o \cdot B} = \frac{0.31}{N_o \cdot B} \tag{2.3}$$

The relationship between received video signal-to-noise to carrier-to-noise, with a 5.7 dB improvement due to NTC 7 weighting, is :

$$SNR = CNR - 1.4 \qquad \text{(dB)} \tag{2.4}$$

2.4 Audio Signal-to-Noise Ratio

The audio signal frequency modulates a carrier that is 4.5 MHz above the visual carrier. The standard frequency deviation is ±25 KHz, and the baseband audio undergoes a standard 75 μs pre-emphasis. The relationship between the unmodulated and modulated bandwidth for an FM signal can be calculated using Carson's rule :

$$B_{ma} = 2 \cdot (\Delta f + B_{ba}) \qquad \text{(Hz)} \tag{2.5}$$

where Δf is the frequency deviation, B_{ba} is the bandwidth of the baseband audio signal, and B_{ma} is the bandwidth of the modulated audio signal. Substituting $\Delta f = 25$ KHz and $B_{ba} = 15$ KHz into equation 2.5, the modulated bandwidth is 80 KHz. Carson's rule tends to underestimate the actual bandwidth, so we will assume a 100 KHz bandwidth for the analysis that follows.

The relationship between signal-to-noise and carrier-to-noise in a FM system (neglecting threshold effects) is given as [5] :

$$\frac{SNR}{CNR} = \frac{3 \cdot \beta^2}{2 \cdot B_{ba}} \tag{2.6}$$

where $\beta = \Delta f / B_{ba}$ is the modulation index, and in this case equals 1.66. The carrier-to-noise ratio in the above equation is calculated in a 1 Hz bandwidth. Substitution into equation 2.6 and converting the result to dBs gives :

$$SNR = CNR - 35 \qquad \text{(dB)} \tag{2.7}$$

Evaluating the noise in a 100 KHz bandwidth and adding 13 dB for improvement due to pre- and de-emphasis [5] gives the final result :

$$SNR = CNR + 28 \qquad \text{(dB)} \tag{2.8}$$

2.5 Multichannel Systems

For more than one channel, each video signal modulates a different carrier frequency, and they are all combined to form a subcarrier multiplexed system (SCM). The standard visual carrier frequencies for cable systems in North America are summarized in Table 2.1.

When more than one channel is sent over a transmission medium, the resulting waveform in the time domain is obtained by application of the superposition theorem. This becomes a very difficult task for a number of signals greater than 2, especially if the signals are uncorrelated. It is important to know the combined peak signal value so that the signal-to-noise ratio can be maximized without distorting the signal due to saturation of the

transmission medium. Worst case addition of all the channels provides a very conservative result because that peak value will be reached a very small percentage of the time, especially for a large number of channels. An appropriate peak value is best found by using numerical time-domain simulations to ensure that all distortion products are less than the design requirement. This approach can only be used if the non-linear characteristics of the system are known or can be approximated. This approach will be used later in this thesis.

Band	**Channel Number**	**Visual Carrier (MHz)**	**Frequency Range (MHz)**
Low	2	55.25	54 - 60
	3	61.25	60 - 66
	4	67.25	66 - 72
	5	77.25	76 - 82
	6	83.25	82 - 88
Mid	14	121.25	120 -126
	15	127.25	126 - 132
	.	.	.
	.	.	.
	22	169.25	168 - 174
High	7	175.25	174 - 180
	8	181.25	180 - 186
	.	.	.
	.	.	.
	13	211.25	210 - 216
Super	23	217.25	216 - 222
	24	223.25	222 - 228
	.	.	.
	.	.	.
	60	439.25	438 - 444
	.	.	.
	.	.	.
	100	679.25	678-684

Table 2.1 - CATV channel allocation in North America

The peak value can also be found by calculating the probability that the composite signal exceeds a certain value. While this approach gives an

indication as to the amount that the signal enters the non-linear regime of a transmission medium, it gives no indication as to the amount of distortion that will be generated. To calculate the peak value using this approach, we consider the addition of N pure sinusoids with equal amplitude A and randomly distributed phases [9]:

$$y(t) = \sum_{i=1}^{N} x_i(t) \tag{2.9}$$

where

$$x_i(t) = A \cdot \sin(\omega_i \cdot t + \theta_i) \tag{2.10}$$

The cumulative probability of the amplitude y exceeding a positive number S (where $S < N \cdot A$) is given by [9]:

$$P(y > S) = \frac{1}{2} - \frac{1}{\pi} \cdot \int_0^{\infty} J_0[(z \cdot A)]^N \cdot [\sin(z \cdot S)] \cdot dz \tag{2.11}$$

Some clarification is needed here, because we are interested primarily in optical transmission systems in which the subcarrier multiplexed signal is used to modulate the intensity (or power) of a light source. Unlike an RF amplifier, which saturates evenly for both positive and negative cycles, the ideal optical transmitter only clips on negative cycles because the intensity of light cannot be negative.

Equation 2.11 is plotted in Figure 2.3 for a varying number of channels. From this graph it is clearly seen that, as the number of channels increases, the probability function has a much smaller variance, and reaches its peak value

(=NA) with a probability approaching zero. It is apparent that the peak value of the modulating signal can be much larger than the linear dynamic range of the transmission medium for a high number of channels, afforded by the fact that this peak value will be reached very infrequently. The percentage of overmodulation allowable in a given system depends on the maximum tolerable in-band distortion that the modulation format can withstand and still deliver the specified signal-to-noise ratio. There is no analytical method to predict this quantity.

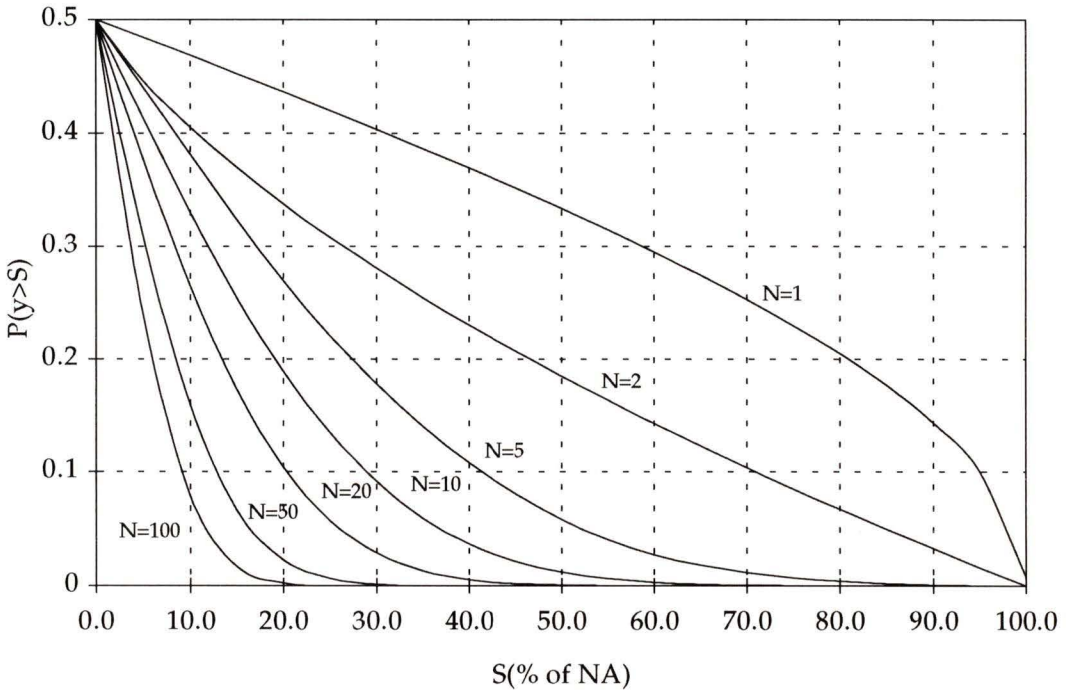

Figure 2.3 - Probability function of multiple channels

Equation 2.11 is plotted again in Figure 2.4 for up to 100 channels. The modulation depth per channel refers to the percentage of the total linear dynamic range of the transmission medium that is taken up by a single channel. $P(m_{tot} > 1)$ is the probability that the composite modulation depth

exeeds the linear dynamic range of the transmission medium on the positive cycle.

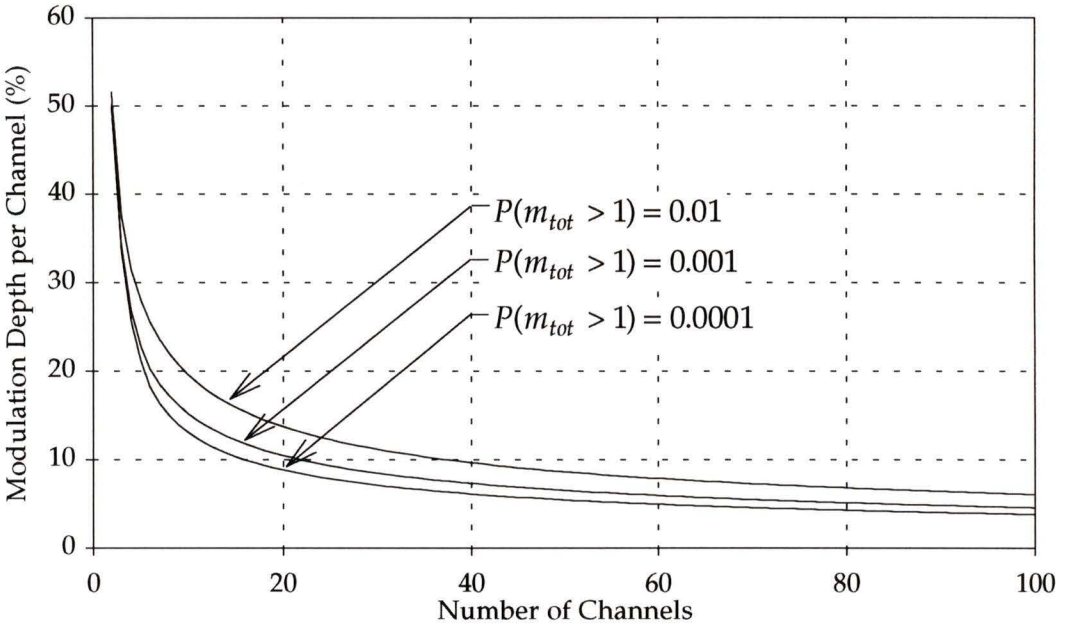

Figure 2.4 - Modulation depth per channel versus number of channels for varying degrees of overmodulation

Amplitude modulated SCM systems are very susceptible to noise and interference because the received signal-to-noise ratio approximately equals the carrier-to-noise ratio, as shown by equation 2.4 for a video signal. The sensitivity of a modulated video signal to an interfering signal depends on the relative frequency of the interfering signal to the visual carrier, as shown in Figure 2.5 [7]. This curve is commonly referred to as the W-Curve, and it indicates the point at which no distortion can be detected, as determined by a subjective audience.

The dominant distortion products in a transmission system are created by 2nd order and 3rd order non-linearities. Higher order distortion products are usually insignificant.

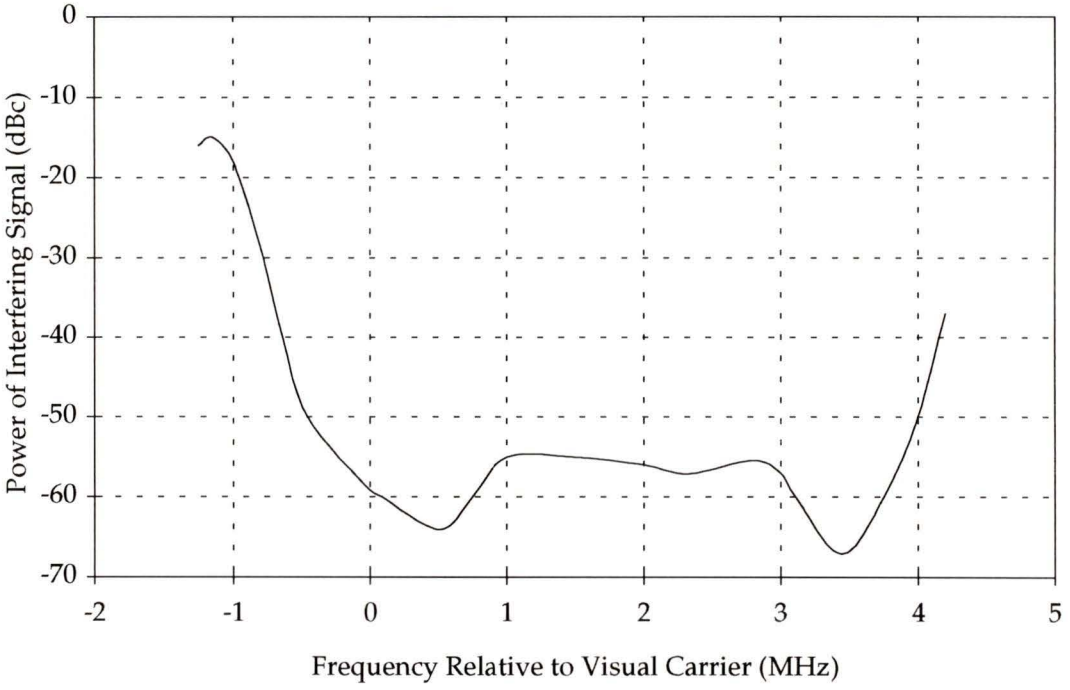

Figure 2.5 - W-curve

2.5.1 2nd-Order Distortion

There are two types of distortion generated by a system with 2nd-order non-linearities; harmonic and intermodulation. The frequencies at which the distortion is generated are given by the following equations:

$$2 \cdot f_1 \qquad \text{(Harmonic)} \qquad (2.12)$$

$$f_1 \pm f_2 \qquad \text{(Intermodulation)} \qquad (2.13)$$

where f_1 and f_2 are arbitrary (but unique) carrier frequencies. The power of harmonic distortion products are 6 dB less than intermodulation distortion products for 2nd-order non-linear systems.

Interference due to second order products is not a problem for single-octave systems because the distortion products fall outside of the transmission bandwidth. For broadband transmission, however, these products cannot be ignored.

Consider a VSB-AM transmission system carrying 100 channels, with the first channel at 121.25 MHz and 6 MHz channel spacings, giving a total transmission bandwith extending from 121.25 MHz to 715.25 MHz. There is only one harmonic product created for every carrier being transmitted. In this example, the harmonic products generated by the first 40 channels fall within the total transmission bandwidth. All of the distortion products are 1.25 MHz above the visual carrier of the channel being interfered with. From the W-curve (Figure 2.5) it is seen that the 2nd-order harmonic distortion created by any carrier must be kept below -55 dBc.

Determining the effect of 2nd-order intermodulation products is not as straightforward because there may be more than one distortion product at a given frequency. It is necessary to total the contribution of each distortion product at each frequency, resulting in the composite second order (CSO) distortion. Figure 2.6 shows a graph of CSO versus frequency for the 100 channel example. The graph shows the amount (in dB) that the composite distortion is greater than a single distortion product at a given frequency.

It is seen that, within the transmission bandwidth, there is a 13 - 19 dB increase in the power of the distortion products due to the addition of multiple distortion products at the same frequency. This, in addition to the fact that intermodulation products are 6 dB greater in power than harmonic

products, shows that 2nd-order intermodulation distortion is the dominant source of interference in multi-octave 2nd-order non-linear systems.

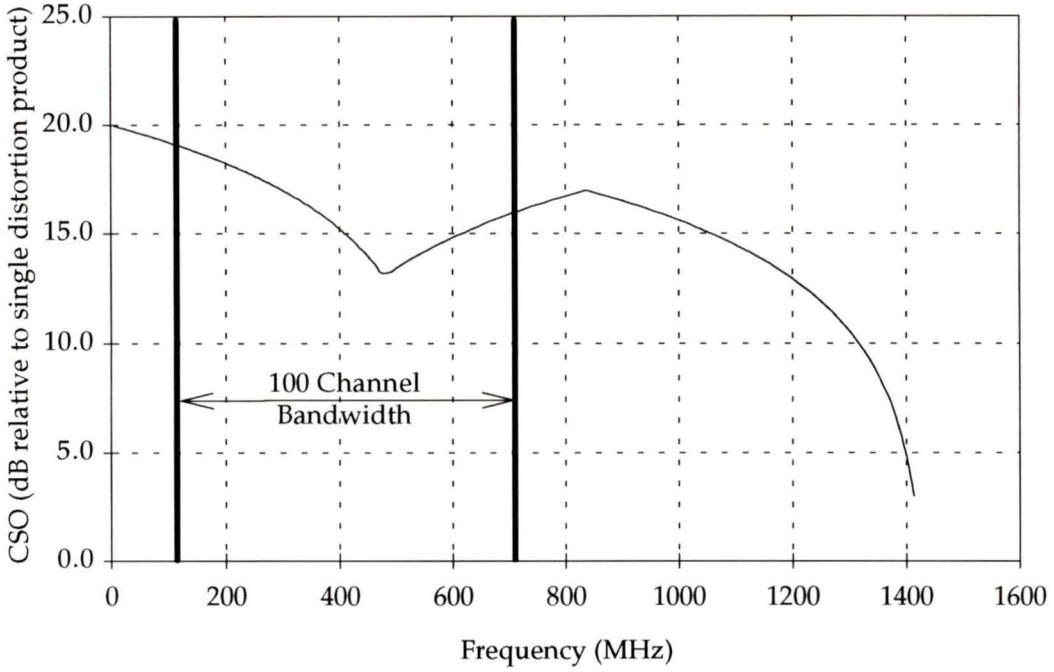

Figure 2.6 - CSO distortion

The CSO distortion products interfere with other channels at two frequencies relative to the visual carrier: -1.25 MHz and +1.25 MHz. The worst-case distortion at these locations and the corresponding sensitivity from the W-curve is summarized in Table 2.2 for a 100 channel system.

It is seen from this table that the modulated video signal is the most sensitive to 2nd-order intermodulation interference at 1.25 MHz above the carrier frequency, and that these products create the most interference in the higher channels. Theoretically, the maximum CSO distortion product within the transmission bandwidth must be 55.0 - (19.0-16.0) = 52.0 dB below the

respective carrier to prevent any noticeable distortion to received video quality.

Frequency of Distortion Product Relative to Visual Carrier (MHz)	Maximum Number of Distortion Products	Channel where Maximum Distortion Occurs	Increase in Distortion Level due to Composite Addition (dB)	Visual Sensitivity from W-curve (dBc)
-1.25	80	1	19.0	-16.0
+1.25	40	100	16.0	-55.0

Table 2.2 - Worst case CSO distortion

2.5.2 3rd-Order Distortion

There are three types of distortion generated by a system with 3rd-order non-linearities: harmonic, combination harmonic/intermodulation (HI), and intermodulation. The frequencies at which the distortion is generated are given by the following equations:

$$3 \cdot f_1 \qquad \text{(Harmonic)} \tag{2.14}$$

$$\left.\begin{matrix} f_1 \pm 2 \cdot f_2 \\ f_2 \pm 2 \cdot f_1 \end{matrix}\right\} \qquad \text{(Harmonic-Intermodulation)} \tag{2.15}$$

$$f_1 \pm f_2 \pm f_3 \qquad \text{(Intermodulation)} \tag{2.16}$$

where f_1, f_2, and f_3 are arbitrary (but unique) carrier frequencies. Intermodulation distortion products generate the most power, followed by HI distortion (6 dB less) and harmonic distortion products (15.5 dB less).

Unlike 2nd-order distortion, which can be neglected for single-octave systems, 3rd-order distortion must be considered for all transmission systems

carrying three or more equally spaced channels because one or more distortion products will fall within the transmission bandwidth.

The number of harmonic distortion products at any frequency will never be greater than one. This is confirmed by equation 2.14. The number of HI distortion products at any frequency will never be greater than N/2, where N is the number of channels. The number of intermodulation distortion products at any frequency varies as N^3 and exceeds 3600 for the 100 channel example cited in the previous section. Intermodulation distortion products are also the most powerful at an individual level and are thus the most dominant source of 3rd-order distortion in subcarrier multiplexed systems.

The composite 3rd-order distortion (commonly known as composite triple-beat, or CTB) is graphed versus frequency for 100 channels in Figure 2.7. It is seen from this graph that the level of distortion within the transmission bandwith is relatively constant, varying by only 3 dB between the centre frequency and the band edges.

The CTB distortion products interfere with other channels at three frequencies relative to the visual carrier: 0, +2.5 MHz, and +3.5 MHz. The worst case distortion at these locations and the corresponding sensitivity from the W-curve is summarized in Table 2.3.

This table shows that distortion products falling at 0 and 3.5 MHz relative to the visual carrier cause the greatest visual degradation to the modulated signal. Theoretically, the maximum CTB distortion product within the transmission bandwidth must be 67 - (35.6-29.4) = 60.8 dB below the respective carrier to prevent any noticeable distortion to received video

quality. This result agrees well with recent publications on this topic [47,51]; however, it is more pessimistic than BP-23 [7], which states that the combination of all 3rd order products lying in a given channel must be less than -53 dBc.

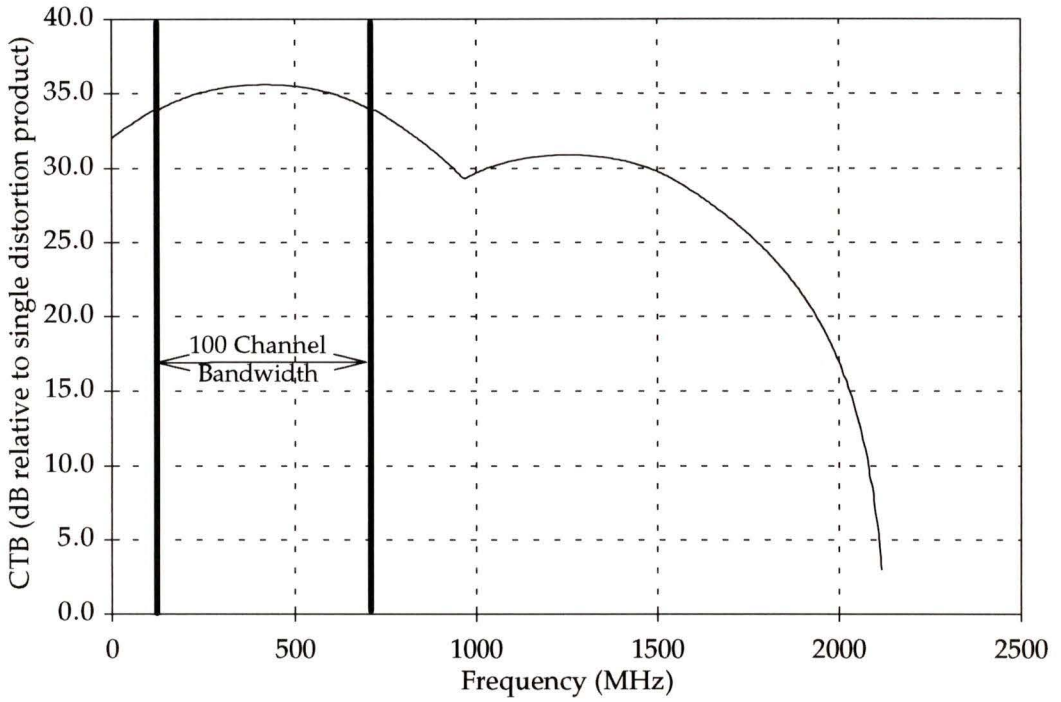

Figure 2.7 - CTB distortion

Frequency of Distortion Product Relative to Visual Carrier (MHz)	Maximum Number of Distortion Products	Channel where Maximum Distortion Occurs	Increase in Distortion Level due to Composite Addition (dB)	Visual Sensitivity from W-curve (dBc)
0.0	3626	50	35.6	-59.5
+2.5	290	100	24.6	-56
+3.5	870	1	29.4	-67

Table 2.3 - Worst case CTB distortion

2.6 Summary

In this chapter the properties of video signal generation, distribution, and transmission have been introduced. Although the subcarrier multiplexed VSB-AM modulation format used for distribution is bandwidth efficient, it is very susceptible to noise and interference, which is a direct result of the received signal-to-noise ratio approximately equalling the carrier-to-noise ratio.

A signal-to-noise ratio of 47 dB is at the threshold of perception for a subjective human audience watching state-of-the-art television sets. For single-frequency interference, such as CSO and CTB distortion, the maximum levels must be less than -52 dBc for CSO and -61 dBc for CTB. The difference arises out of the fact that CSO and CTB create distortion products at different frequencies relative to the visual carrier.

When considering the transmission of multiple channels, it is important to know the peak value of the composite signal so that the carrier-to-noise ratio can be maximized without introducing excessive distortion due to saturation of the transmission medium. As the number of channels increases, the probability of the composite signal reaching its peak value rapidly approaches zero. In a 100 channel system, each carrier can use 4.6% of the linear dynamic range of the transmission medium with a probability of exceeding the linear dynamic range of 0.1%. Although this is a seemingly low probability, it can give rise to significant distortion.

The notion of linear dynamic range, which has a convenient theoretical definition, has no experimental equivalent. In reality, all active transmission

systems distort signals of any level. It is only possible to analytically find the level of distortion introduced by a non-linear system if both the input signal and the transfer characteristic are analytic functions. Where this is not the case, or if the input signal is complex, numerical techniques must be employed. The probabilistic approach used in section 2.5 is only approximate because there is no analytical technique to map the probability of a signal exceeding a certain amplitude to the level of distortion generated by an arbitrary non-linear system.

3. THE FIBRE OPTIC LINK

3.1 Introduction

Figure 3.1 shows the major components of a typical analog fibre optic transmission system. This chapter will introduce these components and explain the fundamental relationships between them at a level required for understanding the remaining chapters of this thesis.

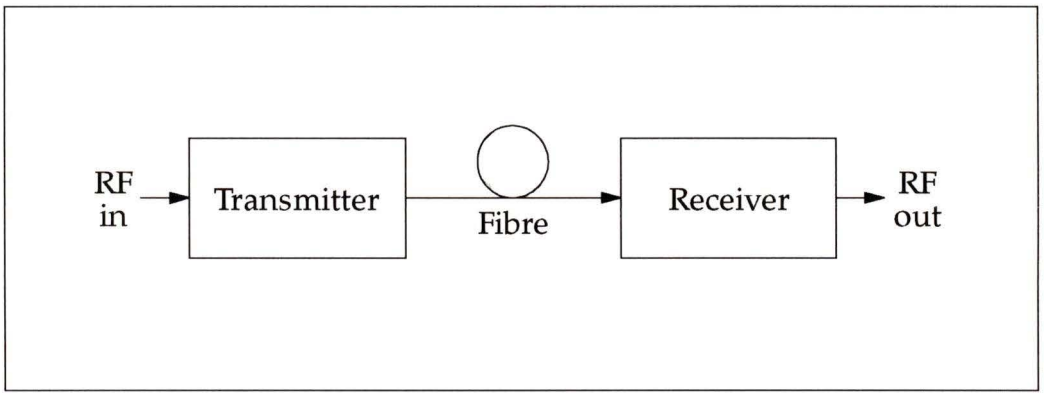

Figure 3.1 - Fibre optic transmission system

3.2 The Transmitter

3.2.1 Laser Diode

The steady-state current-intensity (I-P) relationship of a laser diode is shown in Figure 3.2. The output optical power is essentially zero until the threshold current I_{th} is reached, after which point it increases at a rate proportional to the current. The laser has a specified maximum power output, P_{max}, which should not be exceeded for long term operation. For normal operation the laser is biased at $P_{max}/2$, which allows the greatest swing in optical output

power without clipping. This power is called the average output power or the launch power.

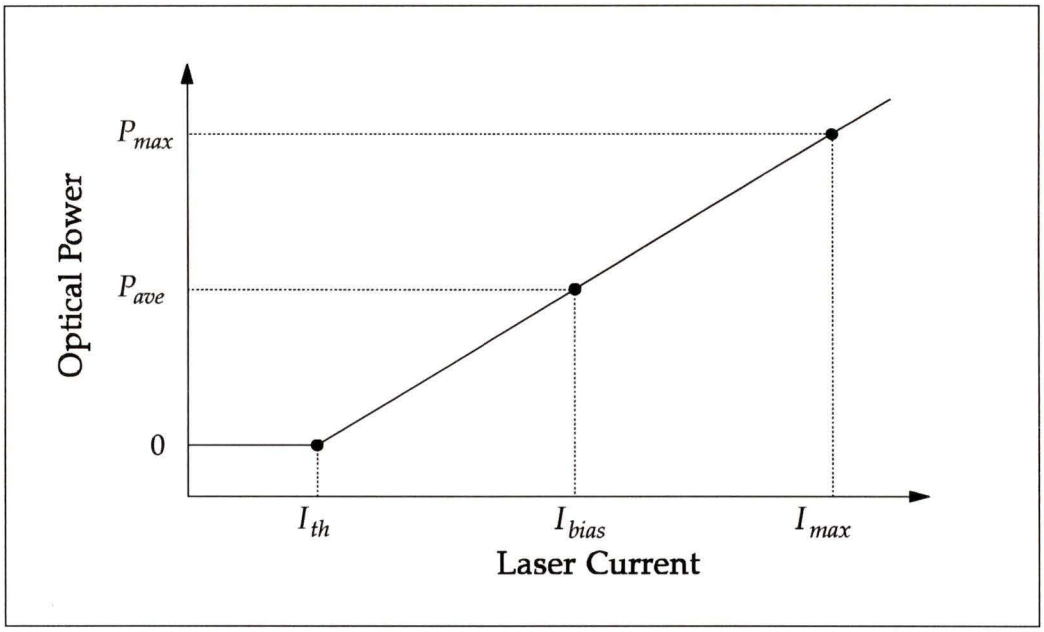

Figure 3.2 - Typical laser diode characteristic

The laser modulation index (depth) is defined as :

$$m = \frac{I_{p-p}}{2 \cdot (I_{bias} - I_{th})} \tag{3.1}$$

where I_{p-p} is the peak-to-peak current swing created by the modulating signal. The modulation index must be less than or equal to unity to avoid clipping.

The optical power versus current characteristic is never exactly linear as is the one shown in Figure 3.2, and thus the laser diode creates harmonic and intermodulation distortion products. There are two types of non-linear distortion created by a laser: static and dynamic. Static distortion results

from a non-linear steady-state transfer characteristic. Such distortion would be apparent from the measured I-P characteristic of a laser. Dynamic non-linear distortion results from a time-varying modulation current. The laser rate equations describe the relationship between input current and output photon density of a laser diode [35, 43]. These equations are coupled non-linear differential equations which must be solved numerically for time-varying modulation currents. From these equations, it can be shown that the level of distortion generated by the laser is a function of both frequency and modulation depth.

The small signal modulation response of a semiconductor laser is also determined by solving the rate equations with a time-dependent current of the form $i(t)=\sin(\omega t)$. The solution shows that the small signal modulation efficiency increases from DC to a maximum, after which it falls off rapidly. The point of peak modulation efficiency is called the relaxation frequency, f_R. This effect is shown in Figure 3.3 [49].

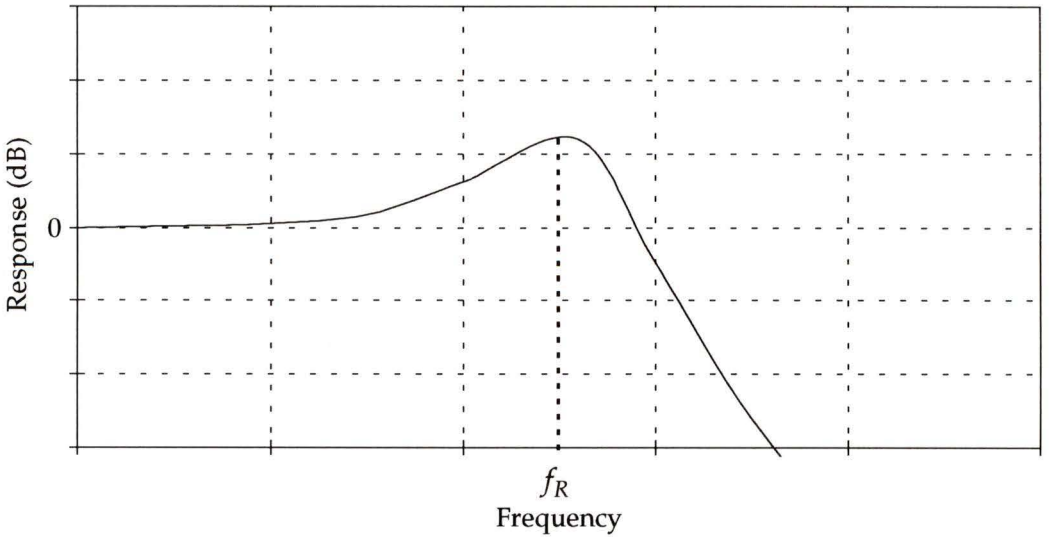

Figure 3.3 - Typical laser modulation response

The modulation response shown is typical for normal bias conditions ($I_{bias} \cong I_{th} \cdot 2$). For higher bias levels, the relaxation frequency f_R increases and the frequency response becomes flatter.

The laser also introduces noise into the transmission system called relative intensity noise, or RIN. As the name implies, this noise level is relative to the light intensity and, in its general form, is given by [34]:

$$RIN = \frac{\left\langle i_{rin}^2 \right\rangle}{I_{rec}^2} \tag{3.2}$$

where $\left\langle i_{rin}^2 \right\rangle$ is the noise power in a 1 Hz bandwidth due to intensity fluctuations of the laser, and I_{rec} is the steady state current in the optical receiver. RIN measurements are usually expressed in terms of photodetector currents in the receiver since this is the first point of signal reception, and it is also a convenient point of reference for other noise sources.

The theoretical lower limit to RIN is given by [3]:

$$RIN_{min} = -10 \cdot \log \frac{\lambda \cdot P_o}{2.48 \cdot q} \qquad \text{(dB/Hz)} \tag{3.3}$$

where λ is the laser wavelength in μm, q is the electronic charge in Coulombs, and P_o is the laser output power in Watts. Equation 3.3 is plotted in Figure 3.4.

Assuming a maximum detector responsivity (at 1.3 μm) of 1.05 A/W, the lowest RIN figure achievable for a 1 mW laser is -155 dB/Hz. For a 10 mW laser, this reduces to -165 dB/Hz. These theoretical minimum values are

difficult to achieve. Most commercially available 1mW Fabry-Perot lasers have RIN figures of -130 to -140 dB/Hz. Distributed feedback (DFB) lasers may achieve RIN figures of -155 to -165 dB/Hz. The laser noise also depends on how much the laser current exceeds the threshold current; closer to the threshold current the relative noise is much higher than at higher current levels and optical powers. The noise also increases with frequency, reaching a peak at the laser relaxation oscillation frequency.

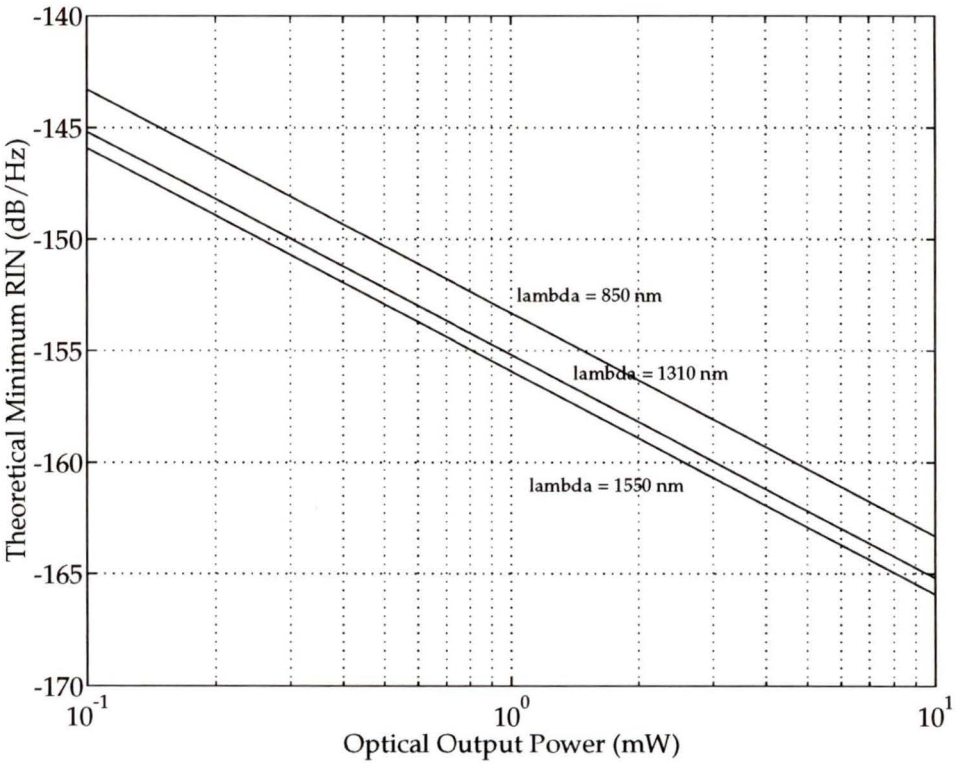

Figure 3.4 - Theoretical RIN versus laser output power

As mentioned previously, it is convenient to reference all noise sources in an optical link to the photodetector current. The photodetector noise current due to the laser is given by :

$$I_{rin}^2 = 10^{\frac{RIN}{10}} \cdot I_{rec}^2 \qquad (A^2 / Hz) \qquad (3.4)$$

where I_{rec} is the steady state received photocurrent.

Another important parameter of lasers is their spectral purity. Fabry-Perot lasers have many modes and inherently wide linewidths. This causes fairly high levels of chromatic dispersion. Alternatively, DFB lasers have very narrow linewidths and are single mode; the light is nearly of a single wavelength.

3.2.2 CW Source and External Modulator

Using a continuous wave (CW) source and an electro-optic modulator (EOM) has several advantages over laser diodes. CW sources in the form of Nd:YAG lasers are commercially available with very high output power (>200 mW), low RIN (<-165 dB/Hz) and narrow linewidth (<10 KHz). In addition, it is possible to use high power Fabry-Perot lasers if the multiple modes and higher RIN can be tolerated. EOMs have a well defined non-linear static transfer characteristic, which is stable with time, and they exhibit no dynamic distortion. There are three main disadvantages to external modulation. The first is that these systems are much more costly and complex than directly modulated laser diodes. The second difficulty with external modulators is that they require a high RF driving voltage. This is difficult to produce in a linear fashion. The final disadvantage is that they have a high optical insertion loss which is typically inversely proportional to the required drive voltage.

A Y-Branch external modulator is shown in Figure 3.5. It is simply the combination of two optical phase modulators. The phase modulator waveguides are fabricated in a crystal, which has the property that the refractive index is proportional to the electric field, thus giving rise to a voltage induced phase shift. Assuming the Y-branch at the input to be ideal, the intensity and phase of the light entering both phase modulator sections is identical. These input waves are represented as complex quantities a_1 and a_2.

$$a_1 = a_2 = \frac{a}{\sqrt{2}} \tag{3.5}$$

The waves at the output of the phase modulator section can be represented in matrix form using common transmission line theory [44]:

$$\begin{bmatrix} b_1 \\ b_2 \end{bmatrix} = \begin{bmatrix} e^{-\alpha L - j\beta(V)L} & 0 \\ 0 & e^{-\alpha L - j\beta(-V)L} \end{bmatrix} \cdot \begin{bmatrix} a_1 \\ a_2 \end{bmatrix} \tag{3.6}$$

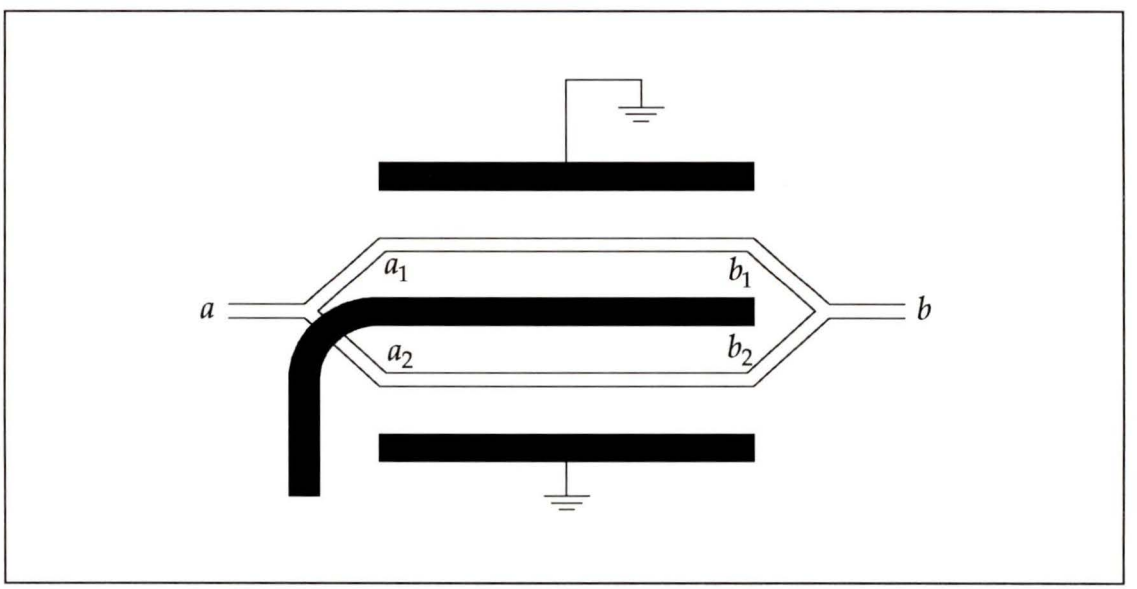

Figure 3.5 -Y-branch external modulator

where b_1 and b_2 represent the output waves, α represents the loss, L is the length of the phase modulators, and β is the propogation constant, which is a linear function of the applied voltage V for Lithium Niobate and Galium Arsenide, the two most commonly used electro-optic materials. Assuming a lossless device and $\beta(V) = V/2$, the intensity (power) transfer characteristic of this device is given by :

$$f(V) = \frac{|b_1 + b_2|^2}{|a|^2} = \frac{1}{2} \cdot [1 - \cos(V)] \tag{3.7}$$

For a device biased at quadrature, there are no even-order distortion products, and equation 3.7 can be re-written as :

$$f(v) = \frac{1}{2}[1 + \sin(v)] \tag{3.8}$$

where v represents a small signal voltage. Equation 3.8 implies that the modulator excess loss is 3dB when no voltage is present on the centre electrode. To achieve this in practice, it is necessary to apply a DC bias on the centre electrode to compensate for manufacturing tolerances and temperature fluctuations. For long term stability of a practical system, it would be necessary to dynamically adjust the bias voltage to maintain the device at quadrature.

The Mach-Zehnder external modulator is similar to the one shown in Figure 3.5, except that the input and output Y-branches are replaced with 3-db optical couplers [27].

3.3 The Fibre

Fibre is generally classified as multi-mode or single-mode. Multi-mode fibre supports many propagating modes. Due to its high dispersion (refer to Section 3.3.3), the present-day use of multi-mode fibre is limited to short-haul applications with low bandwidth requirements. The advantage of multi-mode fibre lies in its cost and its ease of implementation and maintenance.

Single-mode fibre supports only one propagating mode. It offers improved dispersion and loss characteristics compared to multi-mode fibre, and is the fibre employed in long-haul or high bandwidth applications.

3.3.1 Losses

The loss in a fibre optic cable is dependent on the wavelength of the propagating light. The loss also depends to a lesser degree on the physical parameters of the fibre. A typical single-mode fibre exhibits a loss of 0.5 dB/km at 1310 nm and 0.2 dB/km at 1550 nm. These two wavelengths are termed minimum loss windows. Other wavelengths have higher losses due to intrinsic and extrinsic material absorbtion.

3.3.2 Non-linear Effects

Optical fibres do not always behave as linear channels where an increase in incident light intensity gives rise to a proportional increase at the fibre output. Fibre non-linear effects can be classified into two categories: stimulated scattering, and effects arising from the non-linear refractive index of the fibre. Stimulated scattering effects give rise to intensity dependent loss

or gain, whereas the non-linear refractive index is manifested as intensity dependent phase [46].

Stimulated scattering effects are further divided into two mechanisms: stimulated Raman scattering (SRS) and stimulated Brillouin scattering (SBS) [10], both of which result in a loss of energy at the incident frequency and constitute a loss mechanism for optical fibres. The effects of both mechanisms are negligible for incident optical intensity levels up to a threshold value, above which the excess loss increases exponentially. The threshold value represents the maximum optical power that can be coupled to a fibre without significant non-linear distortion.

SBS is a coherent scattering process of light from sound waves [23]. SBS creates a reverse travelling wave (called Stokes light) of a lesser frequency than the incident wave. For incident power levels above the threshold, most of the input light is converted to the reverse travelling Stokes light. The frequency difference between the incident light and the Stokes light is referred to as the Brillouin shift, and is equal to the frequency of the acoustic wave. The shift is about 15 GHz for 1.3 μm light in fused silica fibres. The Brillouin bandwidth or gain profile refers to the variance in the shift frequency. SBS has a threshold of approximately 10 mW for single frequency light in the 1.3 μm window and for fibre lengths > 10 km [23]. Due to the narrow gain profile (≅100 MHz in silica fibre), the incident optical power can be increased past the threshold without penalty by spreading it over a wide frequency range such that no more than the threshold power falls within the gain bandwidth. This implies a source with a spectral density less than 0.1 mW/MHz [11]. This frequency spreading can be accomplished by either

using a source with enough inherent frequency modulation or by external phase modulation.

SRS is similar to SBS, except that Stokes light is generated in both the forward and reverse directions [11]. With SRS, a molecule absorbs a photon at the incident frequency and emits it again at a shifted frequency [49]. Forward travelling Stokes light is generally not a concern for single channel systems where the detector is broadband and there is no selective optical filtering. Unlike SBS, SRS has a much wider gain profile than SBS (≅12 THz in silica fibre [46]) and cannot easily be avoided by spreading the incident optical frequency. Fortunately, the loss threshold of SRS is several orders of magnitude higher than SBS, and equals approximately 1 Watt for a single channel system [45]. For multiple optical channels, the threshold is much smaller and SRS gives rise to crosstalk between channels.

The other main source of fibre non-linearity is due to the non-linear dependence of the index of refraction with optical power density, known as the Kerr effect [49]. This relationship is given by [46]:

$$n = n_o + n_2 \cdot I \tag{3.9}$$

where n is the intensity dependent index of refraction, I is the optical power density, and $n_2 = 3 \cdot 10^{-16}$ cm^2 / W. The Kerr effect gives rise to self phase modulation (SPM) for single channel systems, which causes spectral widening. This could lead to increased dispersion, as described in the following section.

3.3.3 Dispersion

Dispersion refers to the fact that light travels at different velocities down the fibre. A light impulse transmitted from one end of the fibre will be broadened or dispersed after reaching the other end. This phenomenon presents one of the main limitations in the maximum bit-rate that can be transmitted via optical fibre.

In multi-mode fibre, each mode has a unique group velocity. This gives rise to significant dispersion, called intermodal dispersion, and is on the order of 40 ns/km for step index fibres. Graded index fibres can be used to effectively reduce this dispersion down to 0.1 ns/km. Multi-mode fibres also exhibit chromatic dispersion, which is the pulse spreading due to different frequencies of the light source propagating at different group velocities. This source of dispersion is negligible in comparison to intermodal dispersion in multi-mode fibre.

Single-mode fibre does not have intermodal dispersion by the virtue that only one mode propagates down the fibre. The only source of dispersion in single-mode fibre is chromatic dispersion. Chromatic dispersion comprises two components: material dispersion and waveguide dispersion.

Material dispersion occurs because the refractive index of silica is not constant with optical frequency. The material dispersion of silica is zero at 1.276 μm and increases to 20 ps/(km-nm) at 1.55 μm.

Waveguide dispersion occurs because the group velocity of the propagating mode varies with optical frequency. The amount of this variation depends

on several physical properties of the fibre including the core radius and difference in refractive index between core and cladding. These properties are often manipulated such that the waveguide dispersion offsets the material dispersion at a certain wavelength.

The zero dispersion wavelength for typical single-mode fibre with a 8.5 μm core and 125 μm cladding is 1310 nm, which nicely corresponds with a low loss window. It is for this reason that 1310 nm was the commonly used wavelength for fibre optic communications even though the fibre loss at 1550 nm was significantly lower. Today, 1550 nm is the preferred wavelength due to the commercial availability of dispersion shifted fibre.

Dispersive effects in single-mode fibre can be made insignificant by choosing a narrow linewidth source and by operating near the zero dispersion wavelength.

3.4 The Receiver

The optical detector is one of the more ideal components in an optical link. The optical detector is a reverse biased photodiode and can be considered an ideal current source with output current proportional to the light coupled to it. The constant of proportionality is called the responsivity and is given by [6]:

$$R = \frac{\eta\lambda}{1.24} \qquad \text{(A/W)} \qquad (3.10)$$

where η is the quantum efficiency (≤ 1.0) and λ is the wavelength in micrometers. The quantum efficiency of most devices in the 1.3 μm range is 0.8 - 0.9.

In analog applications, the current from the photodiode is converted to a voltage by means of a transimpedance amplifier. This amplifier is typically placed in the same package as the photodiode to reduce parasitic capacitances which degrade frequency response. Non-linearities of the photodetector/pre-amplifier arrangement are dominated by the pre-amplifier, as photodetectors are very linear devices.

The photodetector gives rise to two shot-noise components, one attributable to the dark current and the other due to the received photocurrent. The noise due to the dark current is insignificant in most modern detectors and can be ignored. The noise current due to the received photocurrent from the detector in a 1 Hz bandwidth is given by [42]:

$$I_{det}^2 = 2 \cdot q \cdot I_{rec} \qquad (\mathrm{A}^2 / \mathrm{Hz}) \tag{3.11}$$

where $q = 1.602 \cdot 10^{-19}\,\mathrm{C}$ is the electronic charge.

The pre-amplifier gives rise to its own equivalent noise current, I_{pre}, which is independent of received optical power and can thus be easily measured with the detector diode dark. It is typically on the order of several $\mathrm{pA}/\sqrt{\mathrm{Hz}}$.

3.5 System Performance

The measure of performance of any transmission system depends on the type of signal being transmitted. We are interested only in amplitude modulated

signals as this is the standard distribution method for present-day cable television systems.

Amplitude modulated signals are extremely bandwidth efficient. The modulated bandwidth is only twice that of the baseband signal. This can be further reduced by using vestigial-sideband or single-sideband variations. This thrifty use of bandwidth comes with penalties, however. Amplitude modulated signals are very prone to in-band noise and distortion.

The performance of an optical transmission system is a function of the transmitter, the fibre, and the detector. For most short haul (< 10 km) analog transmission systems, the important performance parameters are the received carrier-to-noise ratio (CNR) and the received intermodulation distortion (IMD).

3.5.1 Carrier-to-Noise Ratio

The received CNR for an optical transmission system is typically calculated at the photodetector output into a reference load. For calculation purposes, it is convenient to reference all signal and noise components as a current in the photodiode.

The small signal current in the photodiode due to a single carrier is given by:

$$I_{rms} = \frac{R \cdot P_{rec} \cdot m_{ch}}{\sqrt{2}} \qquad \text{(A)} \tag{3.12}$$

where R is the responsivity of the photodiode in A/W, P_{rec} is the received optical power in Watts, and m_{ch} is the optical modulation depth of the carrier.

The noise current in the photodiode is calculated from the sum of the noise current contribution from the laser, the photodiode, and the transimpedance amplifier:

$$I_{tot} = \sqrt{I_{rin}^2 + I_{det}^2 + I_{pre}^2} \qquad \text{(A)} \tag{3.13}$$

The CNR in a 1 Hz bandwidth is given by:

$$CNR = 10 \cdot \log\left[\frac{I_{rms}^2}{I_{tot}^2}\right] \qquad \text{(dB)} \tag{3.14}$$

Equation 3.14 is plotted in Figure 3.6 with a noise bandwith of 4.2 MHz and an optical modulation depth of 4.5% per channel (the significance of 4.5% will be explained later in this chapter). From this graph it is evident that the received carrier-to-noise ratio is limited by the laser RIN for high received optical power levels. The benefit of a quiet photodetector is only important for received power levels < -5 dBm.

3.5.2 Intermodulation Distortion

The impact of 2nd and 3rd-order intermodulation distortion on VSB-AM television transmission systems was explained in Chapter 2. It was shown that CSO and CTB distortion products had to be 55 dB and 61 dB below the visual carrier level of any channel to keep the distortion below the threshold of visual perception. For the analysis that follows, we will consider a

transmission system to be suitable for the transmission of VSB-AM video if the maximum IMD product is less than -60 dBc.

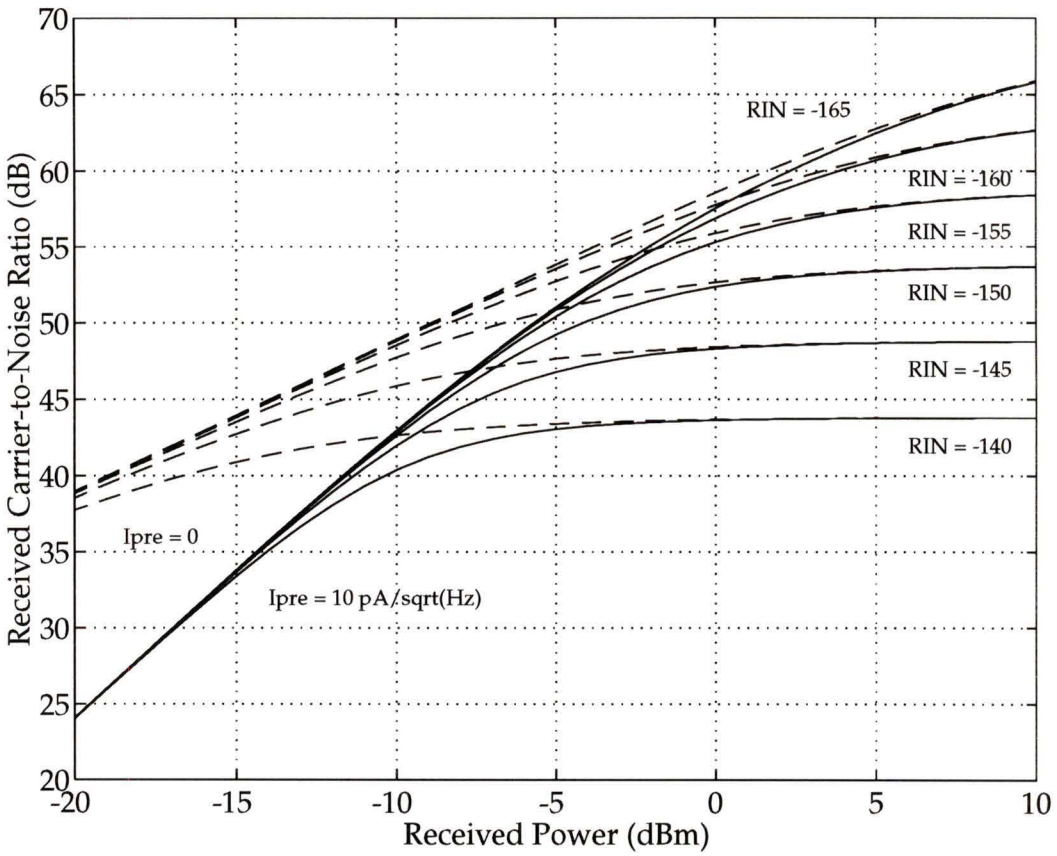

Figure 3.6 - CNR versus received optical power

To establish a baseline with which to compare different linearization schemes, the maximum optical modulation depth (OMD) per channel is determined for a linear optical transmission system carrying 100 channels. Numerical solutions are obtained by creating a time-domain vector containing 100 channels with uniformly distributed phases, with a sampling frequency an order of magnitude greater than the highest frequency component. This vector is then applied to a linear transfer characteristic similar to that shown in Figure 3.2 for different modulation depths, and the

result is Fourier transformed using a 65536 point FFT. A gradient-based search algorithm is used to find the modulation depth which corresponds to the desired level of distortion.

Using the above simulation technique, it is found that a maximum modulation depth per channel of 4.5% can be used on a 100 channel linear optical transmission system while maintaining distortion levels less than -60 dBc. The resulting frequency spectrum is plotted in Figure 3.7.

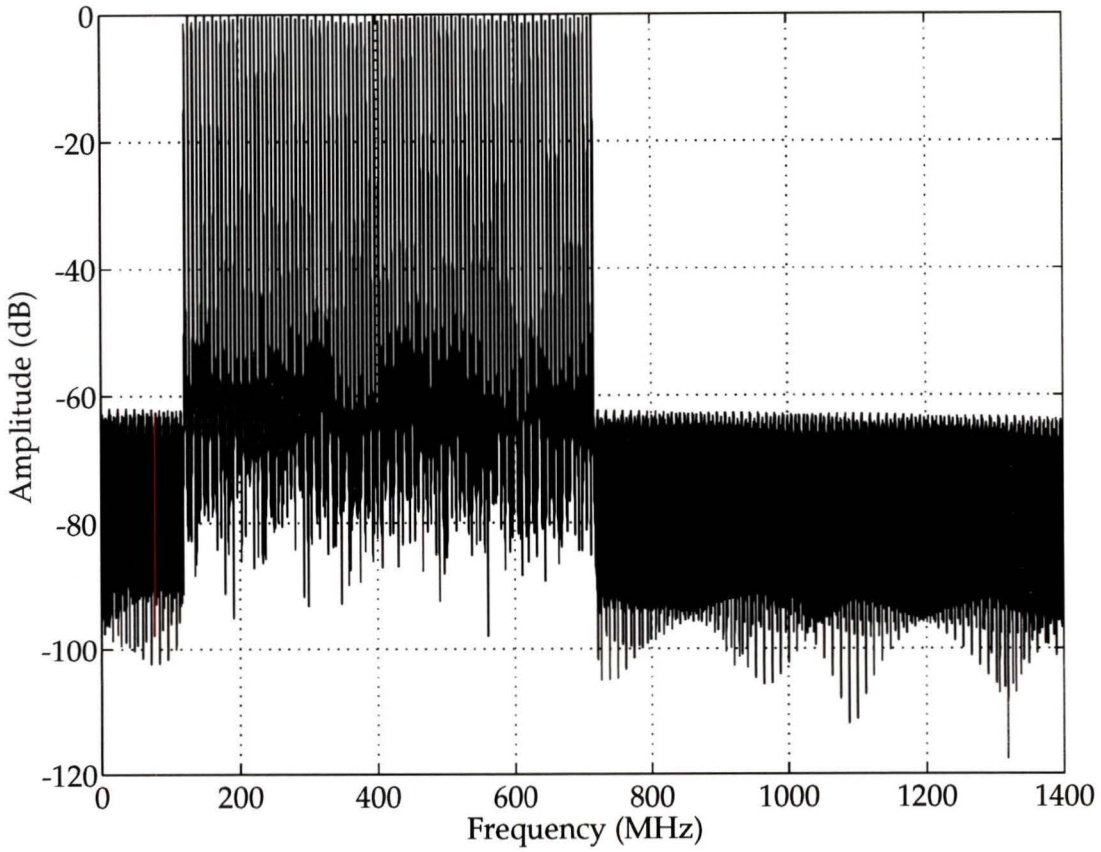

Figure 3.7 - Frequency spectrum of 100 channel system

All of the distortion in Figure 3.7 is a result of clipping the negative cycle of the modulating signal. From Figure 2.5 it is seen that a theoretical maximum modulation depth of 4.5% for a 100 channel system corresponds to a probability of exceeding the linear dynamic range of the laser diode of approximately 0.1%.

Overmodulation of the laser is not the dominant source of distortion in practical systems carrying a large number of channels. Other system non-linearities such as static and dynamic laser non-linearities or the non-linear transfer characteristic of EOMs usually generate an intolerable level of distortion prior to overmodulation becoming a problem.

4. LINEARIZATION TECHNIQUES

This chapter discusses the advantages and disadvantages of various schemes for linearizing optical transmission systems. All methods presented focus on extrinsic linearization, i.e. linearization of a non-linear optical system by manipulating either the electrical or optical signal. The schemes discussed are equally applicable to systems with directly modulated laser transmitters or with externally modulated CW sources. No attempt is made to discuss intrinsic linearization of the various components that comprise the optical transmission system. The advantages and disadvantages of each method will be discussed for both directly modulated laser systems and externally modulated systems. Many of the methods discussed here are also applicable to RF amplifier linearization.

4.1 Pre-Distortion

A block diagram of the pre-distortion method is shown in Figure 4.1. A non-linear network with an inverse non-linear transfer characteristic to that of the optical transmission system is placed prior to the laser diode or electro-optic modulator. While conceptually simple, this method is very difficult to implement.

The non-linear pre-distortion network must be designed to exactly match the distortion characteristics of the optical transmission system. For directly modulated laser diode systems, this is an extremely difficult task for several reasons. Firstly, the non-linear characteristics of every laser diode are different, and thus the pre-distortion network must be tuned to the individual laser diode. Secondly, the non-linear characteristics of laser

diodes change over time. This dictates that the pre-distortion network must be adaptive to match the ever changing characteristics of the laser. The third and most important reason why pre-distortion linearization techniques are difficult to implement is that the amplitude and phase of the distortion produced by a laser diode is frequency dependent. This makes it virtually impossible to design a wide-band pre-distortion network capable of matching the laser's characteristic over the useful frequency response of the laser.

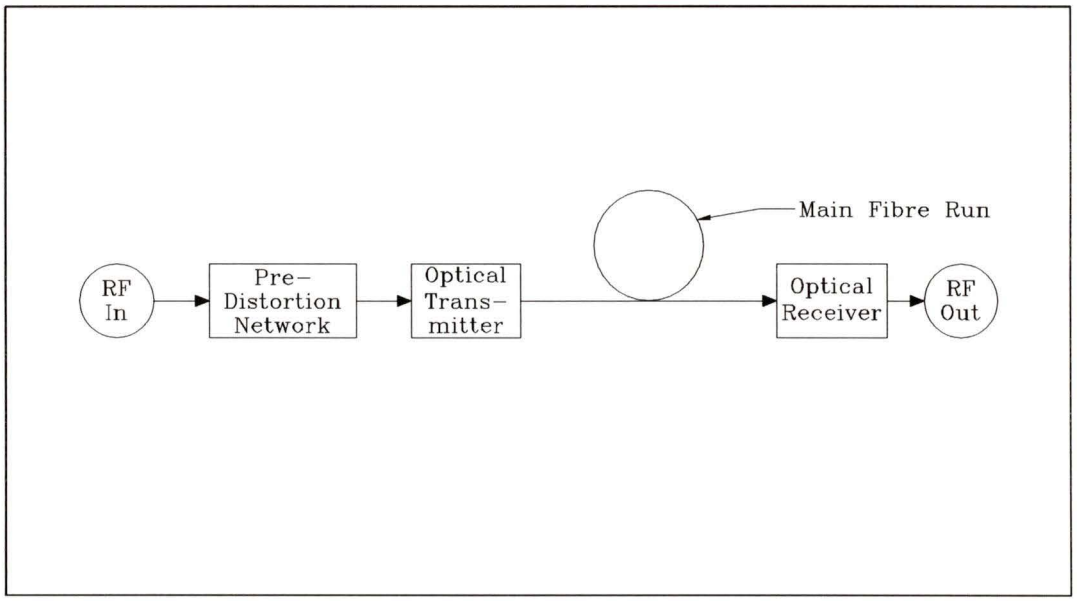

Figure 4.1 - Pre-distortion linearization

The use of pre-distortion for externally modulated systems is much more feasible. The three reasons given above for directly modulated laser diodes are not applicable to externally modulated systems, due to the fact that they are passive devices. Externally modulated transmission systems are also easier to linearize using pre-distortion because they generate only odd-order distortion products when biased at quadrature. This means that the pre-

distortion network need only generate odd-order distortion products, which can be easily accomplished with balanced circuit configurations. The non-linear transfer characteristic of an EOM is very stable with frequency due to the fact that it is a passive device. Any pre-distortion network will contain active components, which are very difficult to make work properly over several octaves. This fact generally limits the use of pre-distortion linearization of EOMs to narrow bandwidth systems.

There is no improvement in system noise performance with pre-distortion linearization.

4.2 Feedforward

Optical feedforward is shown schematically in Figure 4.2 for a laser diode system. As the name suggests, this system generates an error signal by comparing the original signal to be transmitted to a sample of the actual signal being transmitted. This error signal is then used to modulate a second laser which 'adds' the necessary amount of light necessary to linearize the output. Unlike pre-distortion, this linearization is adaptive and does not rely on a known non-linear transfer characteristic of the optical transmission system.

Theoretically, feedforward transmission is the most effective linearization technique. Depending on the non-linear characteristics of the optical transmitters used in the system, the optical coupling ratios k_1 and k_2 can be optimized to maximize linearity and reduce RIN. Using the 100 channel example cited in Chapter 2, a theoretical optical modulation depth of 3.5%

per channel can be used with Mach-Zehnder modulators. This is theoretically better than the Quasi-Feedforward method (refer to section 4.3).

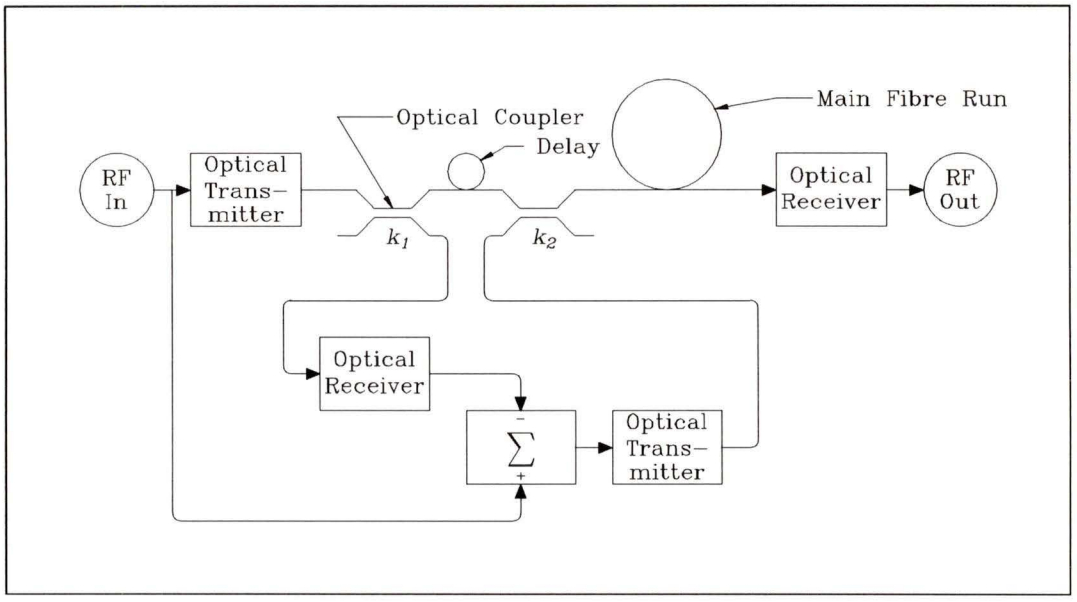

Figure 4.2 - Feedforward linearization

There are several disadvantages to the feedforward technique. Two optical sources of different wavelengths are required. The light from these sources propagates down the fibre at different velocities due to dispersion. In order to obtain the maximum linearization, the group delay of the light from the compensating laser must exactly match that of the main laser so that the two sources reach the photoreceiver at the same time. This requires that the feedforward transmitter be optimized for a certain transmission distance, or that the wavelength separation between the main laser and compensating laser is sufficiently small to make the differential group delay negligible.

The feedforward technique is also very complex, requiring two optical sources, two receivers, and an assortment of electrical and optical splitters

and amplifiers. Furthermore, all of these devices must be amplitude and phase matched over several octaves.

An additional advantage of feedforward linearization is that noise reduction can also be achieved via the secondary transmitter which cancels the RIN generated by the primary transmitter. This approach is only effective if the coupling ratio k_2 is low or if the secondary transmitter has low RIN. The noise performance of a feedforward system, when using CW lasers and EOMs, is limited by the RIN of the secondary transmitter due to the fact that the coupling ratio is quite high ($k_2 = 27\%$) in order to achieve maximum linearity. A more thorough analysis of feedforward applications using directly modulated laser diodes can be found in [35].

4.3 Quasi-Feedforward

Quasi-feedforward is a linearization technique that uses a non-linear system with identical characteristics to that of the main optical transmission system to pre-distort the RF signal prior to transmission. Unlike pre-distortion, where the RF signal is distorted by passing it through a non-linear network with an inverse transfer characteristic to that of the transmission system, this method relies on the creation of the pre-distorted signal by means of subtracting the distortion components created by a parallel non-linear system with matched distortion characteristics. A block diagram of this approach is shown in Figure 4.3.

This scheme has been used to linearize LEDs with limited success [1]. There are several disadvantages to this scheme when using it to linearize LEDs or

laser diodes. The scheme relies on the two optical transmitters to have matched non-linear characteristics over a wide bandwidth which is very difficult to achieve in practice. This scheme (as shown in Figure 4.3) also provides no RIN reduction of the optical transmitter; in fact, it reduces the carrier-to-noise ratio by a minimum of 3 dB due to the fact that the two optical paths are essentially in series.

Because quasi-feedforward is essentially a pre-distortion scheme and requires no optical couplers, it is possible to use a single light source and two electro-optic modulaters as the transmitters. This approach offers savings in complexity and also allows significant noise reduction of the optical source. This approach is discussed in detail in the following chapter.

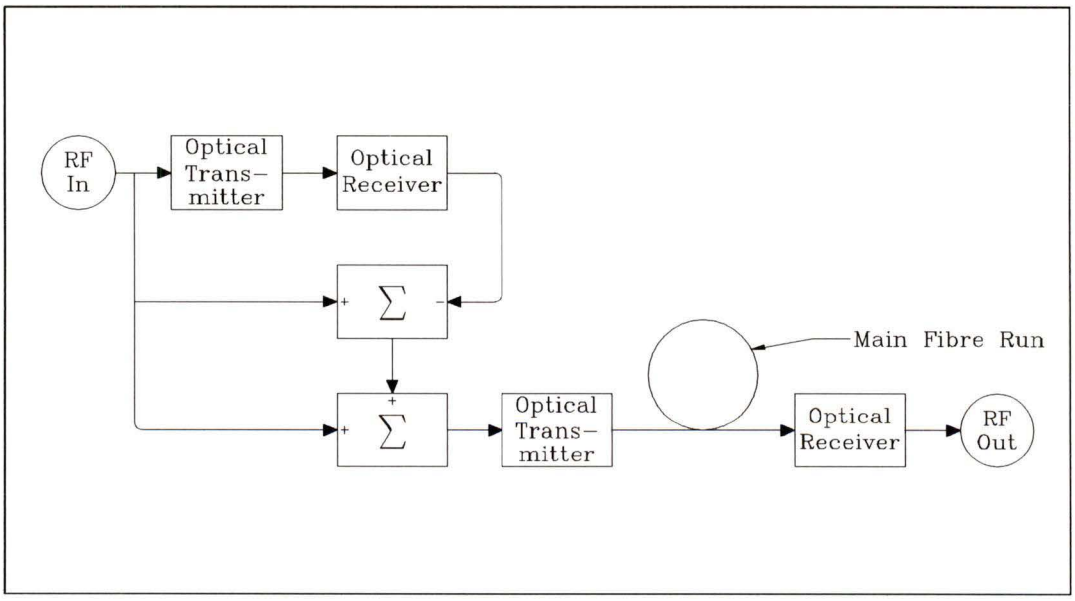

Figure 4.3 - Quasi-feedforward linearization

5. THEORETICAL PERFORMANCE OF QUASI-FEEDFORWARD LINEARIZATION

5.1 Introduction

In this chapter the quasi-feedforward (QFF) linearization scheme will be examined for use with externally modulated transmitters. This arrangement has several advantages over other linearization schemes such as reduction in laser RIN, a single optical source, and a power budget limited only by the optical source and fibre non-linearities.

5.2 Description

The proposed scheme is shown in Figure 5.1. For the analysis that follows, we assume each EOM is a standard Mach-Zehnder type biased at quadrature. In this configuration, there are no even-order distortion products and the transfer characteristic is given by equation 3.7, which is repeated here for convenience:

$$\frac{P_{out}}{P_{in}} = 1 + \sin(V) \tag{5.1}$$

where V is the applied voltage. Consider an RF input signal $2\sqrt{2}s$ at point i in Figure 5.1. Assuming the gain G_{h-d} = 0 dB, the signal at point d is:

$$V_d = \sin(s) \tag{5.2}$$

The signal applied to the second modulator is thus:

$$V_e = 2s - k \cdot \sin(s) \tag{5.3}$$

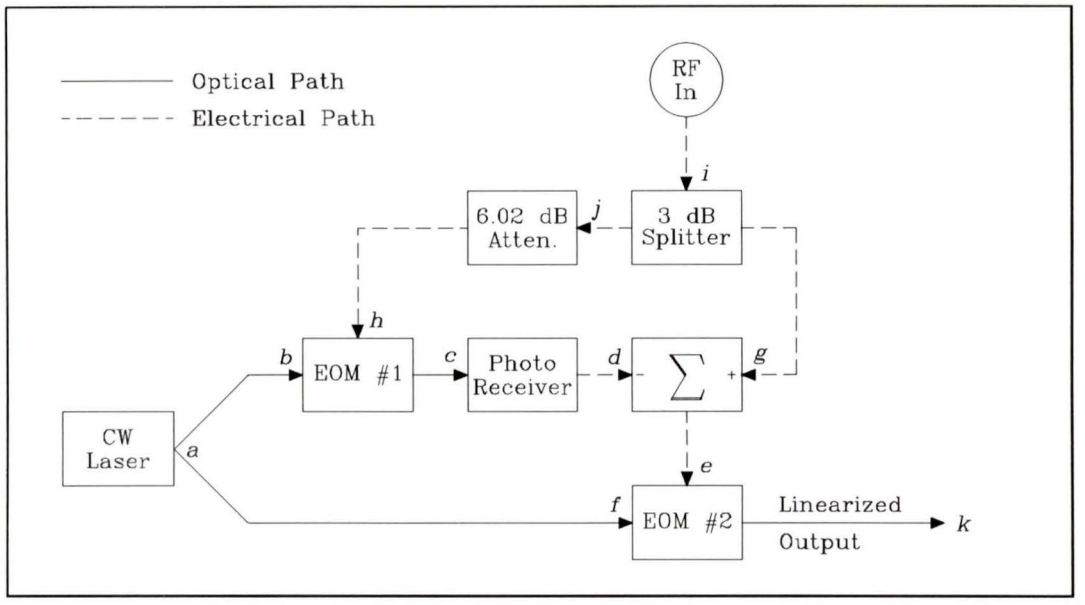

Figure 5.1 - Quasi-feedforward block diagram

with $k = 1$. This requires the group delay in path *i-g* to equal that in path *i-d*. Equation 5.3 represents the original RF signal plus the distortion products generated by EOM #1 added 180° out of phase. This signal is then input to the second EOM, whose output in terms of the original RF input signal is:

$$f(s) = \frac{P_{out}}{P_{in}} = 1 + \sin[2s - k \cdot \sin(s)] \tag{5.4}$$

Equation 5.4 represents the transfer function of the QFF linearization scheme with standard Mach-Zehnder modulators. This equation is an odd function, and hence the linearized modulator does not introduce even order distortion products. The constant k in equations 5.3 and 5.4 is nominally set to $k = 1$. This corresponds to the case of:

$$\left.\frac{\partial^3 f}{\partial s^3}\right|_{s=0} = 0 \tag{5.5}$$

The value of k can be optimized further to obtain even lower composite distortion by increasing the 3rd order products slightly and reducing the 5th order products. The case of $k = 1$ will be used in this thesis as it provides a convenient means of experimental calibration. In addition, the small difference in the optimized value would be difficult to realize in a practical implementation. This is discussed further in Section 5.4. Equations 5.1 and 5.4 are plotted in Figure 5.2. It is seen that the QFF transfer characteristic is more linear than that of the standard EOM.

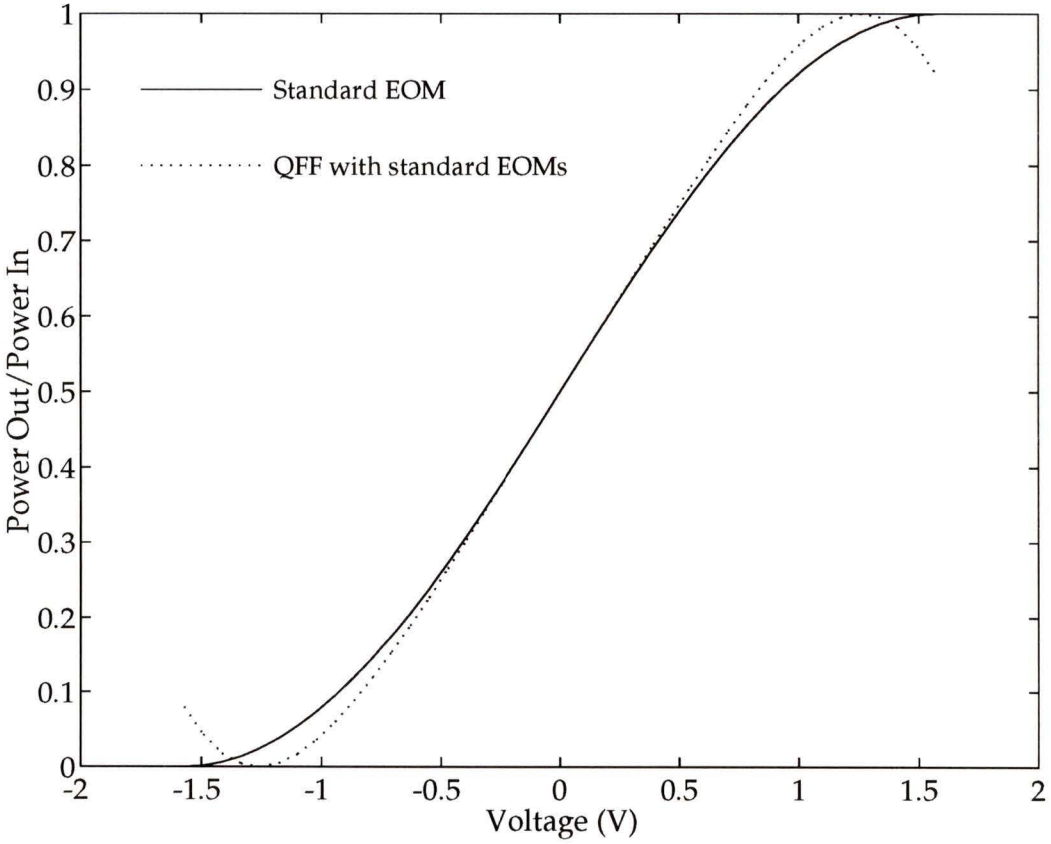

Figure 5.2 - Power transfer characteristic of standard EOM and QFF system employing standard EOMs

Time domain simulations with 100 CW carriers show that a maximum peak modulation depth of 2.2% per channel can be used while maintaining distortion levels below -60 dBc (Figure 5.3). This represents an increase of 1.5% per channel over that of a single EOM, and results in an improved receiver CNR as described in section 5.3.

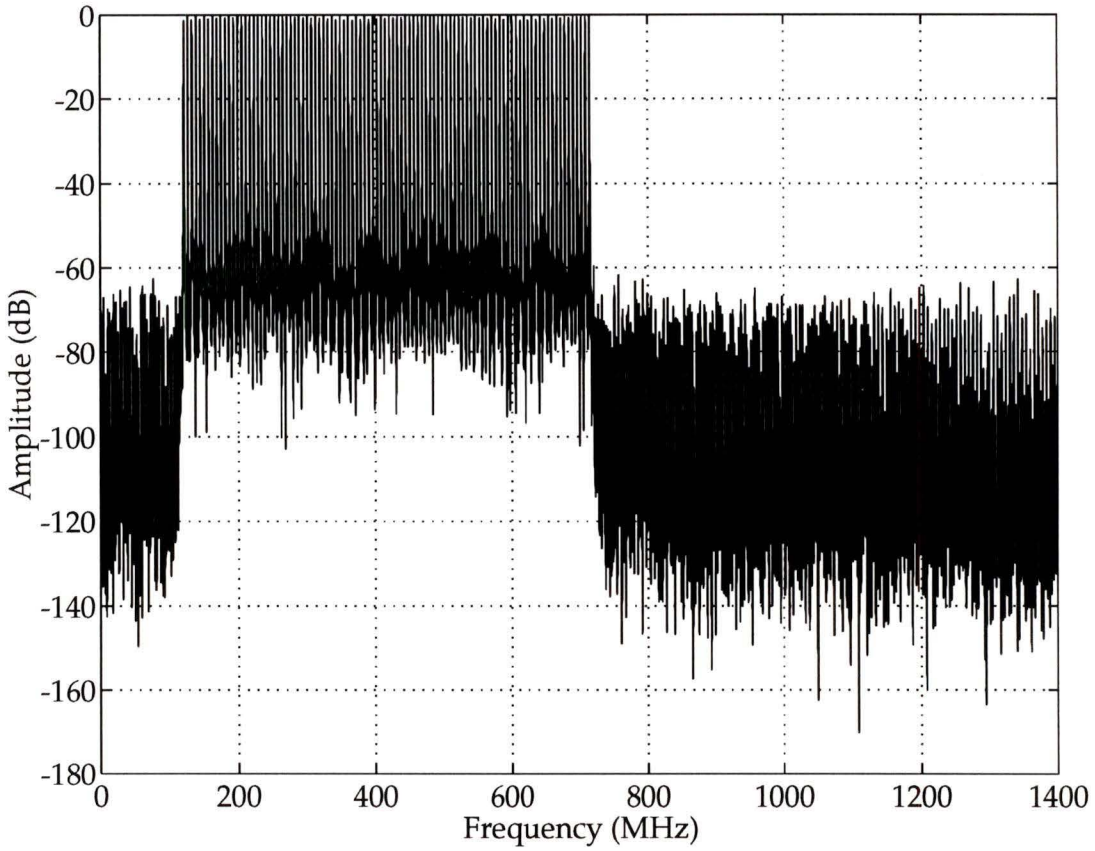

Figure 5.3 - Output spectrum of QFF system employing standard EOMs. 100 CW channels at standard CATV frequencies. OMD = 2.2%/channel.

We now consider the case of using a linearized modulator, shown schematically in Figure 5.4 [2]. This modulator is created by cascading a Y-Branch and Mach-Zehnder modulator. It should be noted that there are

many variations of this type of linearized modulator, all of which offer similar performance.

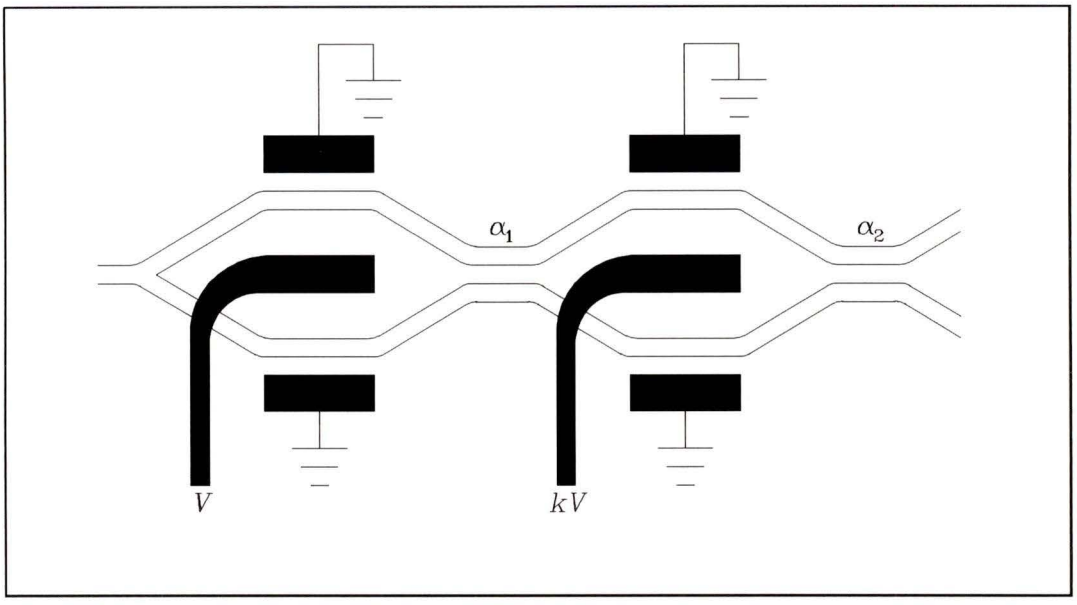

Figure 5.4 - Linearized cascade modulator

The 4-port transformation matrix of this modulator is given by [2]:

$$T = T_{c2} \cdot T_{p2} \cdot T_{c1} \cdot T_{p1} \tag{5.6}$$

where the two input ports are after the first Y-branch. The transformation matrix $T_{c1,2}$ of the couplers is given by:

$$T_{c1,2} = \begin{bmatrix} \cos(\alpha_{1,2}) & -j \cdot \sin(\alpha_{1,2}) \\ -j \cdot \sin(\alpha_{1,2}) & \cos(\alpha_{1,2}) \end{bmatrix} \tag{5.7}$$

The transformation matrices of the phase modulator sections are:

$$T_{p1} = \begin{bmatrix} e^{jV} & 0 \\ 0 & e^{-jV} \end{bmatrix} \tag{5.8}$$

$$T_{p2} = \begin{bmatrix} e^{jkV} & 0 \\ 0 & e^{-jkV} \end{bmatrix} \tag{5.9}$$

Assuming an ideal Y-branch at the input, the amplitude and phase of the light entering each arm will be identical, and the power transfer characteristic between the input port and either of the output ports is given by:

$$f(x) = |T_{11} + T_{12}|^2 \tag{5.10}$$

By optimizing the ratio of drive voltages between the modulators (k) and the coupling ratios of the two couplers (α_1, α_2) for minimum composite third-order distortion by using a gradient search algorithm, it is found that:

$$\alpha_1 = \alpha_2 = 27^\circ \tag{5.11}$$

$$k = -0.5 \tag{5.12}$$

Substituting equations 5.7 to 5.9 into equations 5.6 and 5.10 yields the transfer characteristic of this linearized modulator:

$$\begin{aligned} \frac{P_{out}}{P_{in}} = 1 &+ 3.24 \cdot \cos^2(V)\cos(\frac{V}{2})\sin(\frac{V}{2}) \\ &- 1.90 \cdot \cos^2(\frac{V}{2})\cos(V)\sin(V) \\ &- 1.62 \cdot \sin(\frac{V}{2})\cos(\frac{V}{2}) \end{aligned} \tag{5.13}$$

When this modulator is used in a quasi-feedforward arrangement, the transfer function is shown in Figure 5.5 along with that of a linearized MZ modulator (equation 5.13) and a conventional modulator without linearization. This figure shows the enhanced linear region of the QFF system.

Time domain simulations with 100 CW carriers show that a maximum peak modulation depth of 3.6% per channel can be used while maintaining distortion levels below -60 dBc (Figure 5.6). This compares very favourably to the maximum modulation depth of 4.5% per channel with linear modulation of 100 channels.

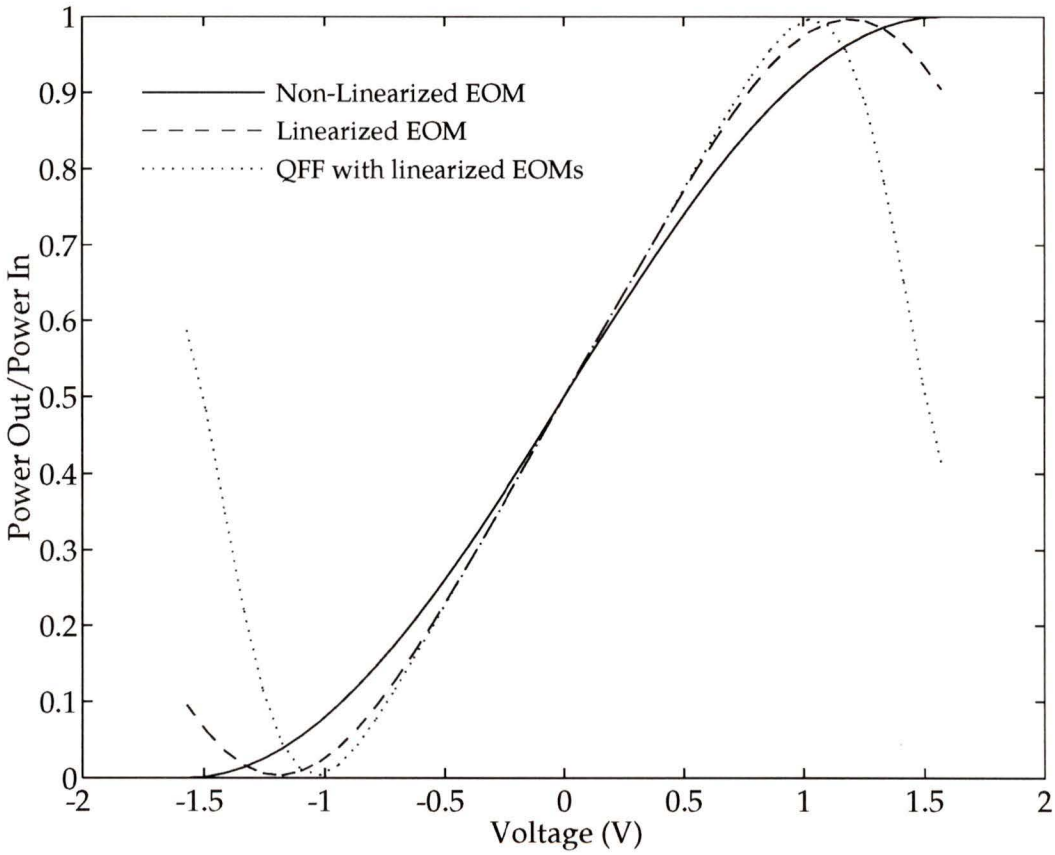

Figure 5.5 - Power transfer characteristic of linearized EOM and QFF system employing linearized EOMs

5.3 Noise Analysis

The noise performance of this scheme is evaluated by calculating the output noise power of the first modulator/detector pair and adding it through the

non-linear transfer characteristic of the second modulator. This is difficult to do theoretically because the laser RIN cannot be considered as Additive White Gaussian Noise (AWGN). The noise contribution due to RIN at the receiver output is proportional to the instantaneous received optical power. We have used computer simulations to calculate the carrier-to-noise ratio for various conditions of laser RIN and optical modulation depth.

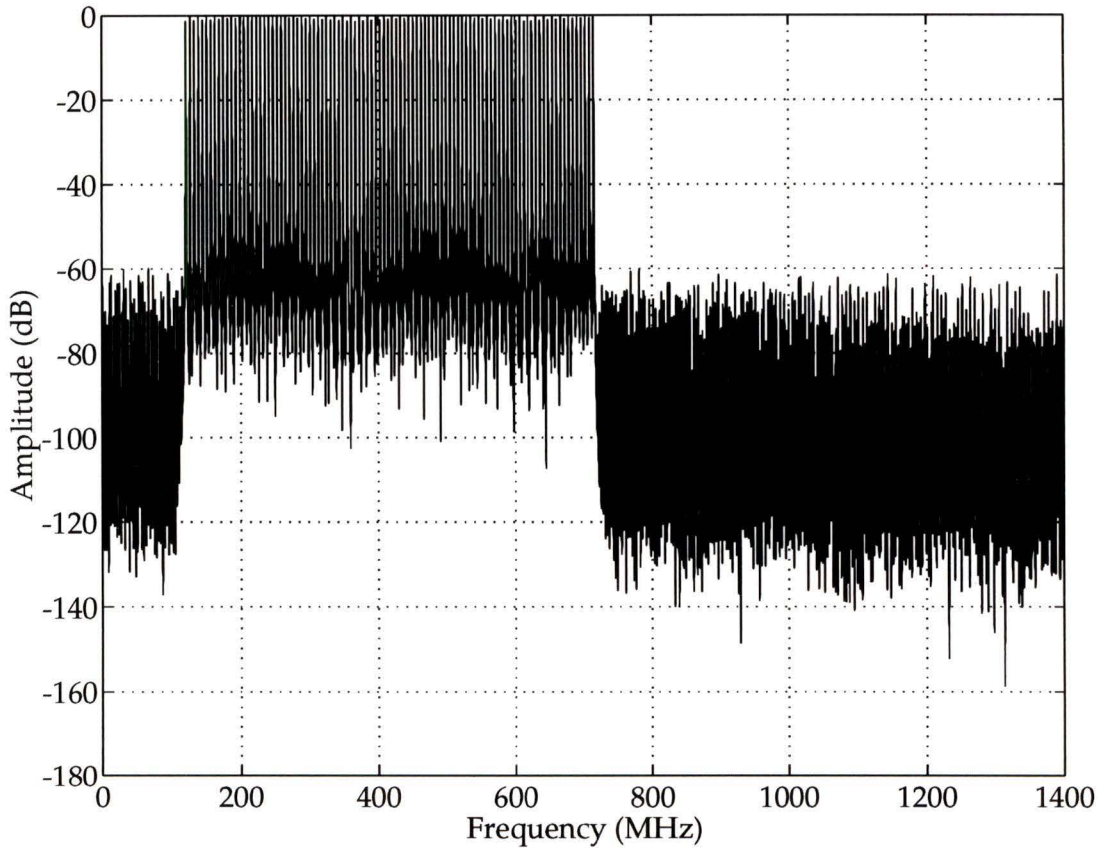

Figure 5.6 - Output spectrum of QFF system employing linearized EOMs. 100 CW channels at standard CATV frequencies. OMD = 3.6%/channel.

By matching the group delay in paths *a-e* and *a-f* in Figure 5.1, it is possible to partially cancel the laser RIN by ensuring the phase of electrical signal at point *e* is such that the RIN noise component is 180° out of phase with the

optical RIN at point *f*. Intuitively, if the above conditions are met, the RIN will be cancelled almost entirely for small optical modulation depths where the modulators are essentially linear. For larger modulation depths, however, the non-linear effects of the modulators reduce the amount of cancellation. This effect is shown in Figure 5.7 for both standard MZ modulators and the linearized MZ modulators. It is seen that the RIN improvement for practical levels of optical modulation depth (2.2% for standard EOMs, 3.6% for linearized EOMs) is 33.2 dB and 34.1 dB, respectively.

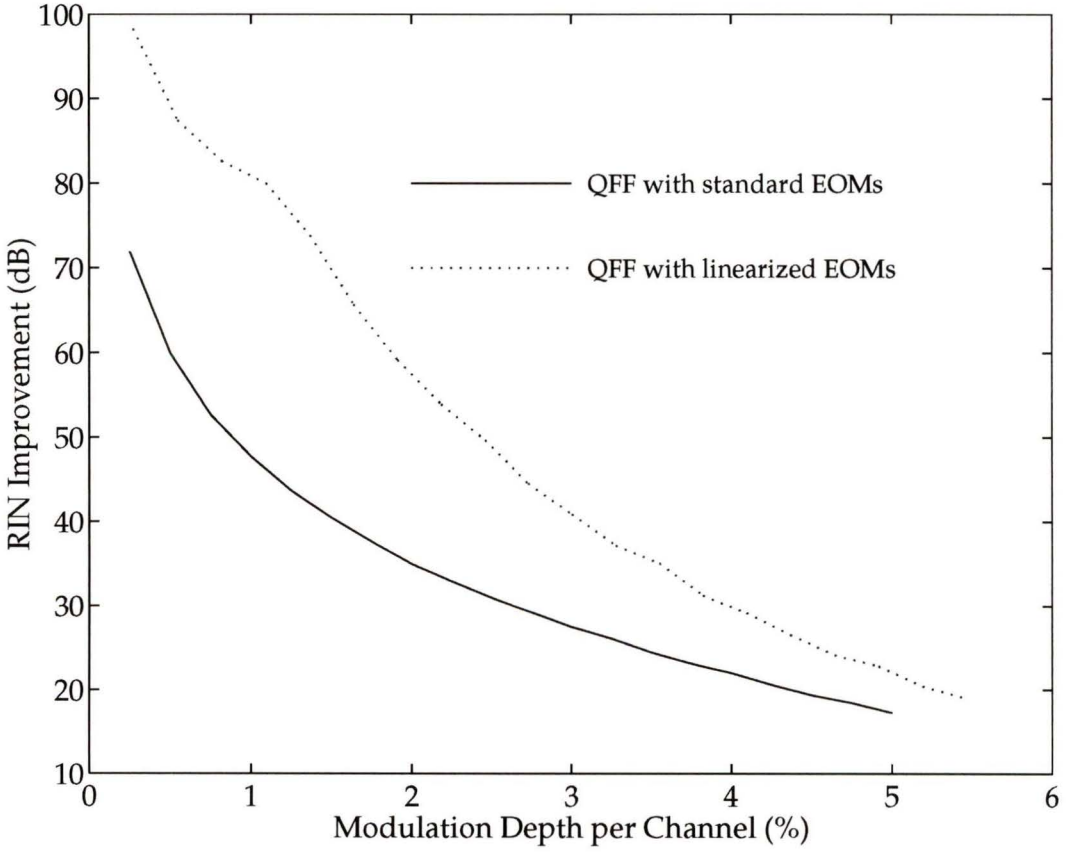

Figure 5.7 - Improvement in RIN versus optical modulation depth for 100 CW channels

CNR versus RIN for 4 different cases is shown in Figure 5.8. The first case is a single standard EOM with 0.7% modulation depth, this being the maximum for a 100 channel system meeting CSO and CTB requirements. The second case is QFF with standard MZ EOMs and 2.2% modulation depth. The third case is QFF with linearized MZ EOMs and 3.6% modulation depth. The final case is a perfectly linear modulator with 4.5% modulation depth. This represents the theoretical upper limit to CNR for a received optical power of 0 dBm and a pre-amplifier noise of 10 $pA/\sqrt{Hz}$, without noise cancellation. We can see from this graph that the CNR for the quasi-feedforward schemes reaches a maximum at a RIN of approximately -130 dB/Hz. The implication of this is that there is no point in using an optical source with a RIN of <-130 dB/Hz with quasi-feedforward linearization, as there will be no further improvement in receiver carrier-to-noise ratio. This fact makes this scheme attractive for use with inexpensive Fabry-Perot lasers with high ouput power and relatively high noise.

Figure 5.9 shows the ratio of carrier-to-noise ratios at the outputs of the two photoreceivers in the QFF schemes. It is seen that the two CNRs are identical at a RIN of approximately -153 dB/Hz. Thus for lasers with a RIN less than –153 dB/Hz there is a penalty in noise performance which stems from the fact that the two optical links are essentially in series. The maximum penalty of 3 dB occurs when there is no laser RIN. For example, if a source with a RIN of -175 dB/Hz were used with a conventional modulator and with QFF linearized modulators, the CNR at the output of the conventional system would be 3 dB higher than the QFF linearized system. This demonstrates that QFF linearization imposes a slight noise penalty when used with low noise optical sources.

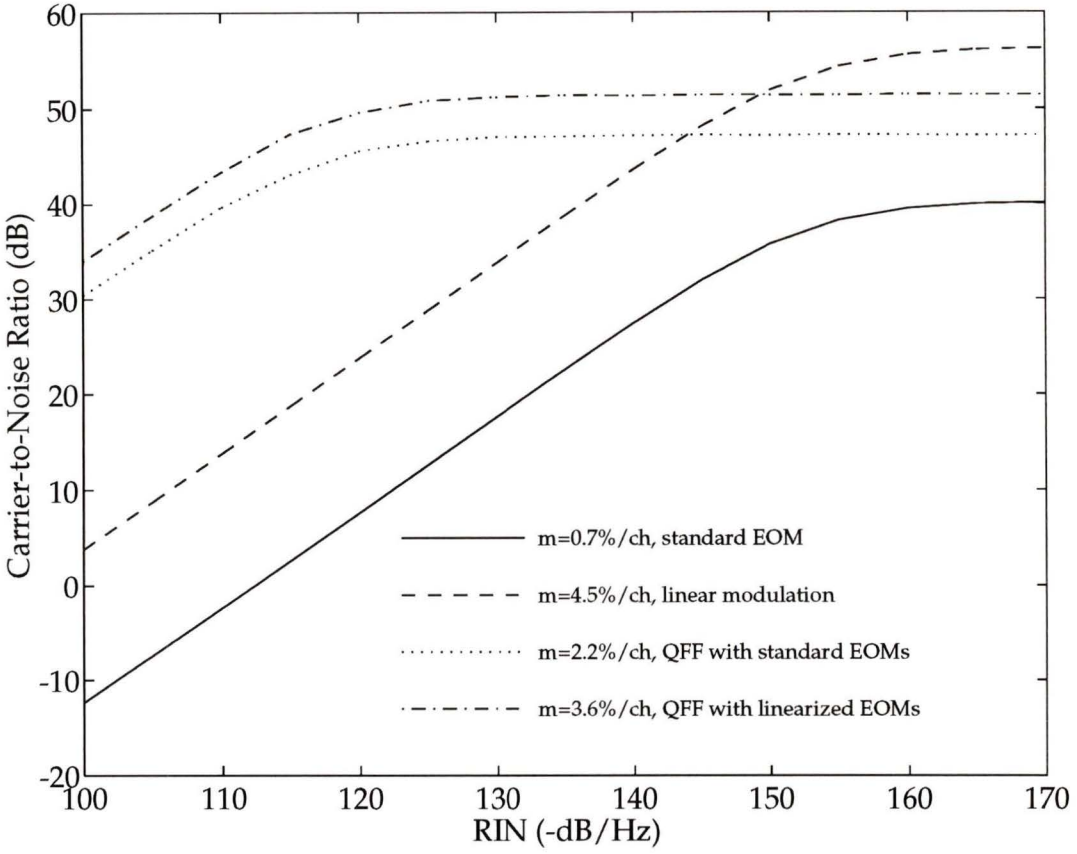

Figure 5.8 - Carrier-to-noise ratio versus RIN for various transmitters. Noise bandwidth = 4.2 MHz, received optical power = 0 dBm, pre-amplifier noise = 10 pA / $\sqrt{\text{Hz}}$.

5.4 Tolerance Analysis

In this section we analyze how system non-idealities affect performance. In a practical system, non-perfect amplitude and phase responses of the various components will degrade system performance. We look at the effect of a non-ideal error signal in terms of both the phase and amplitude imbalance at the combiner. A contour plot of this is shown in Figure 5.10 for the case of QFF with standard modulators. The amplitude error corresponds to

deviations of k from unity in equations 5.3 and 5.4. It can be seen that the minimum distortion occurs at an amplitude imbalance of -0.18 dB and a phase imbalance of 0°. It is also seen that a maximum amplitude error of approximately 0.5 dB and a maximum phase error of ±2° (at the maximum frequency of 715.25 MHz) can be tolerated while maintaining distortion levels below -60 dBc.

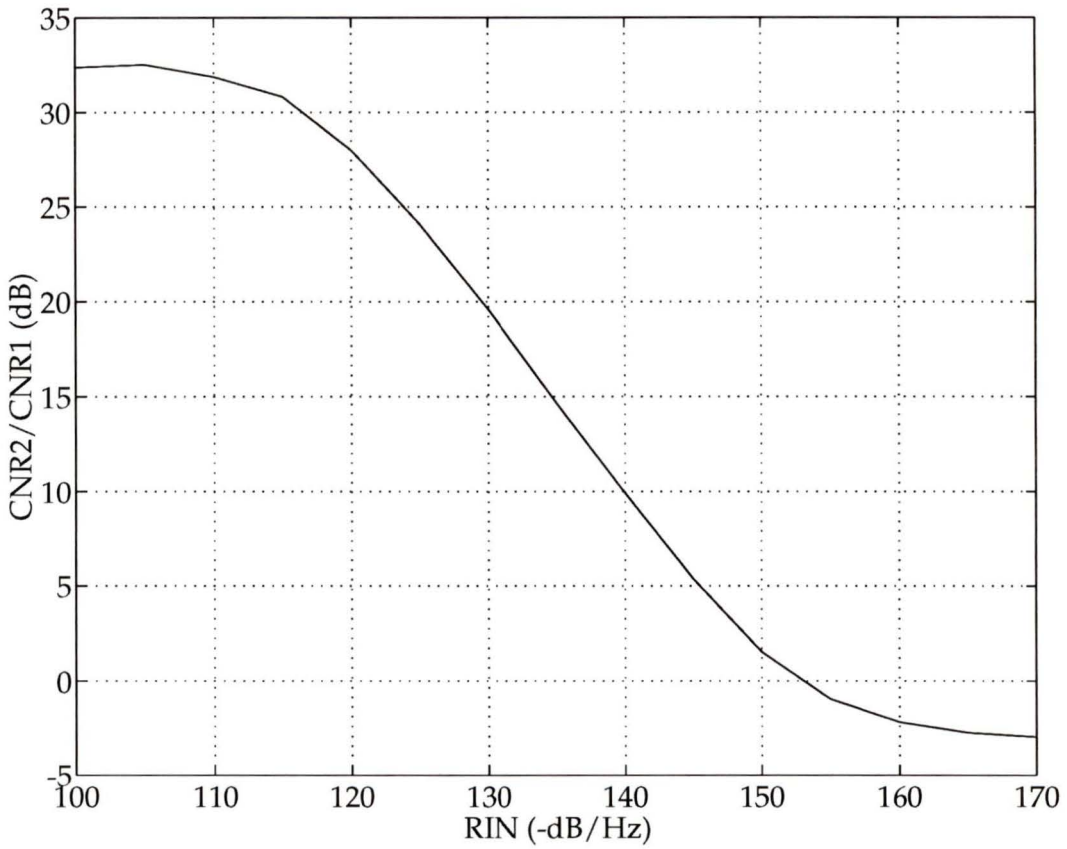

Figure 5.9 - Improvement in CNR at linearized output over CNR at output of EOM #1.

A similar plot for RIN cancellation is shown in Figure 5.11 for a 100 channel QFF system with standard modulators. The amplitude error again corresponds to deviations of k, and the phase imbalance corresponds to

differences between the paths *a-e* and *a-f* in Figure 5.1 (at 715.25 MHz). We see that the amount of RIN cancellation is much more sensitive to phase imbalance than amplitude imbalance.

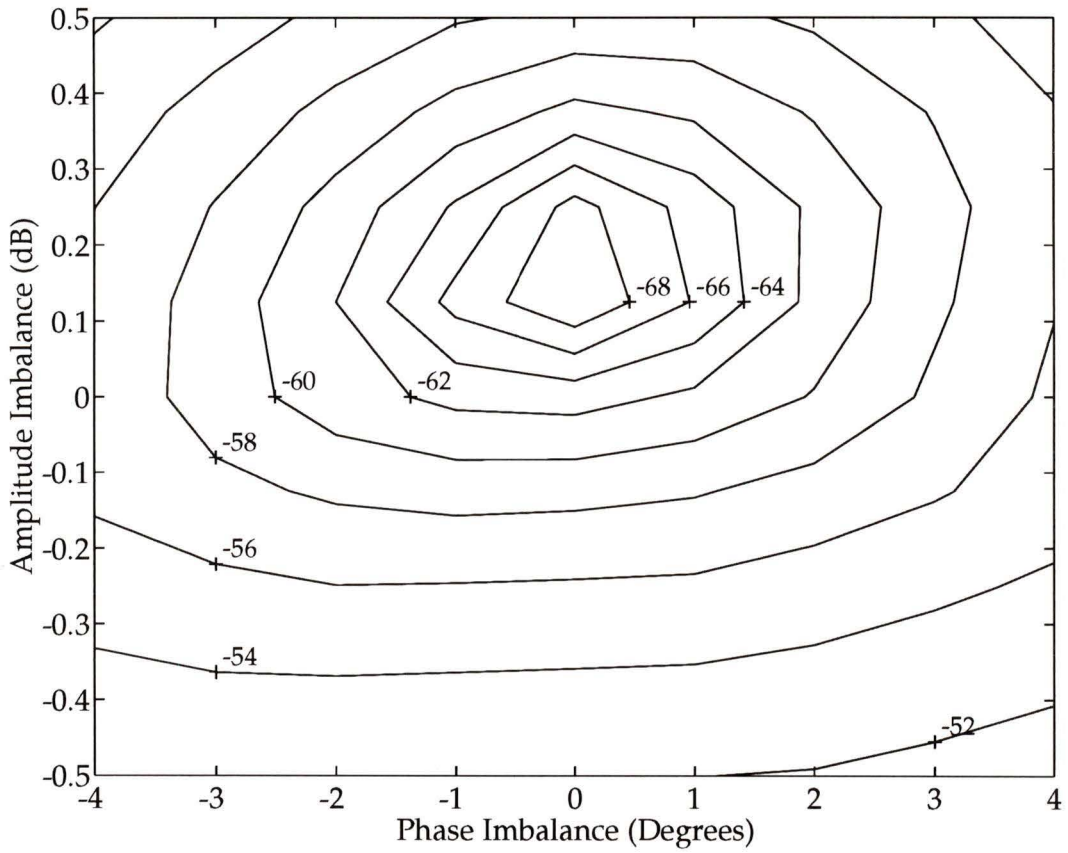

Figure 5.10 - Distortion versus phase and amplitude imbalance for QFF with standard EOMs. 100 CW channels, OMD = 2.2%/channel.

5.5 Conclusions

It this chapter, we have discussed a new linearization scheme for externally modulated systems. Theoretical simulation results have shown that this technique is suitable for high capacity CATV systems operating with relatively noisy CW lasers. A tolerance analysis has shown that in order to

make the system perform satisfactorily, a high degree of amplitude and phase matching must be obtained over the entire bandwidth of the system.

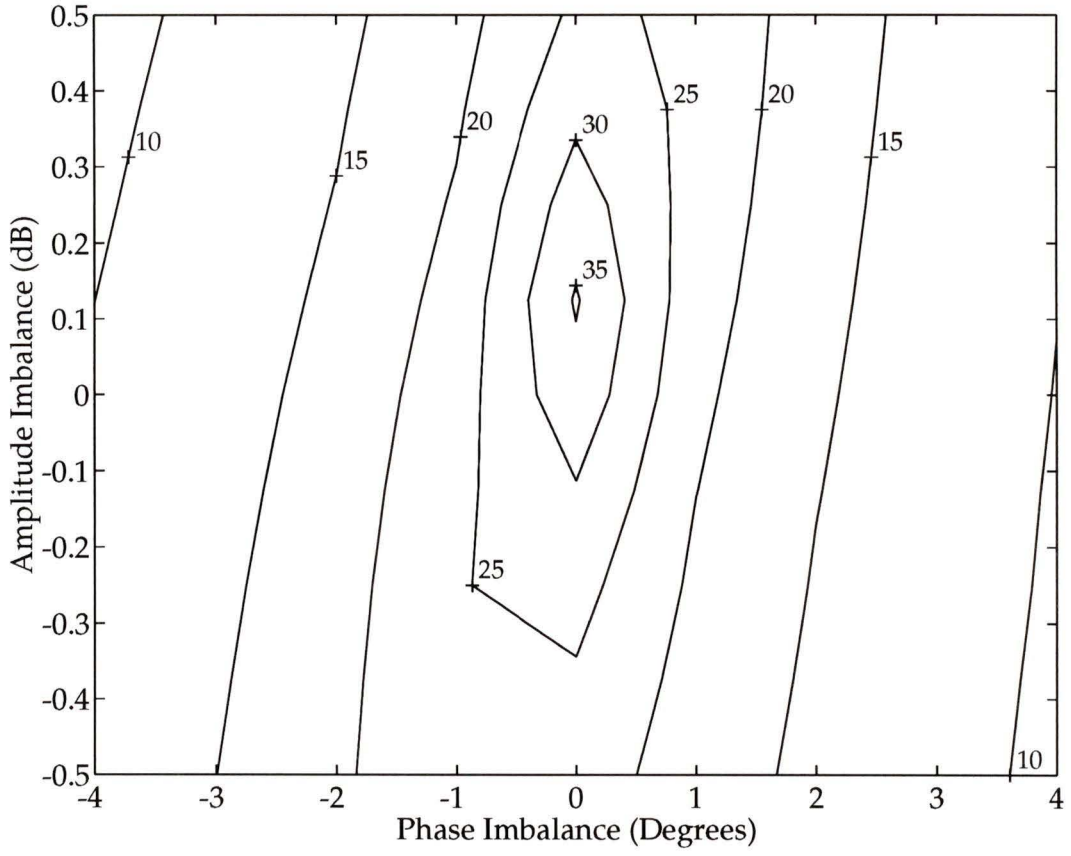

Figure 5.11 - RIN improvement versus phase and amplitude imbalance for QFF with standard EOMs. 100 CW Channels, OMD = 2.2%/channel

Quasi-feedforward linearization of external modulators has the advantage of increased power budget due to the availability of high power CW optical sources. In addition, the quasi-feedforward scheme is simple enough to be integrated onto a single substrate.

6. MEASURED PERFORMANCE OF QUASI-FEEDFORWARD LINEARIZATION

6.1 Introduction

This chapter experimentally verifies the simulated results of the quasi-feedforward linearization scheme presented in Chapter 5. This validation is accomplished using a high power CW laser and standard electrooptic modulators. The experimental setup could not be tested with the high number of carriers used for the simulations of the previous chapter due to the lack of necessary test equipment. In lieu of this, measured S-parameters were used from the experimental system to numerically simulate system performance for 100 channels.

It is noted that no attempt was made to experimentally verify the RIN reduction available with this linearization scheme. This is due to the fact that the CW laser being utilized has a very low RIN (<-165 dB/Hz), and hence no improvement would be possible.

6.2 Experimental Setup

The theoretical analysis of Chapter 5 predicted that a good amplitude and phase match between the optical and electrical paths of a quasi-feedforward system is essential in order to obtain satisfactory performance. It is a relatively simple matter to obtain a flat amplitude and linear phase response on electrical path *i-g-e* in Figure 5.1, as there is only a splitter, coaxial delay, and combiner in this path. The optical path *i-j-h-c-d-e* is more difficult due to the EOM and photodetector in this path. In addition, the optical path requires some electrical gain which is not shown in Figure 5.1. In this

experiment, the amplitude and phase response of the optical path were extremely poor in the frequency range of interest due to the EOMs. Figure 6.1 and Figure 6.2 show the amplitude and phase response of the two EOMs from 40 MHz to 1 GHz. It is seen that, while the match between the EOMs is good, the amplitude varies by 5 dB and the phase by 20° over the 1 GHz bandwidth. This poor response is partly attributable to the fact that the modulators are designed for from 1GHz up to 8 GHz.

In order to obtain a usable 100 channel bandwidth, channels 2-6 in the low band (refer to Table 2.1) were not used, and the first channel was taken to be at 121.25 MHz, which eliminates the worst portion of the EOM response. The uppermost channel was taken to be 715.25 MHz, which leaves room for 100 carriers at a 6 MHz channel spacing.

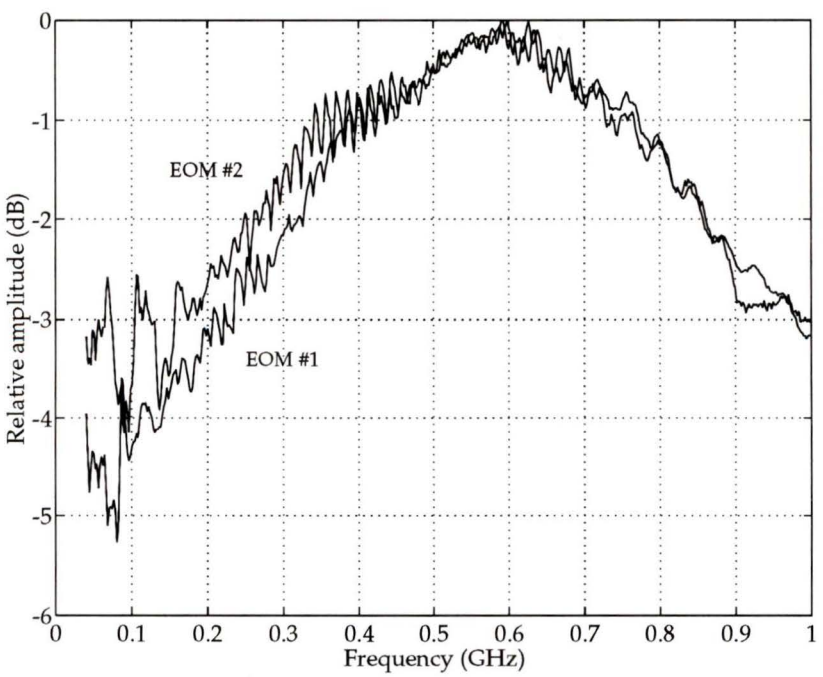

Figure 6.1 - EOM frequency response

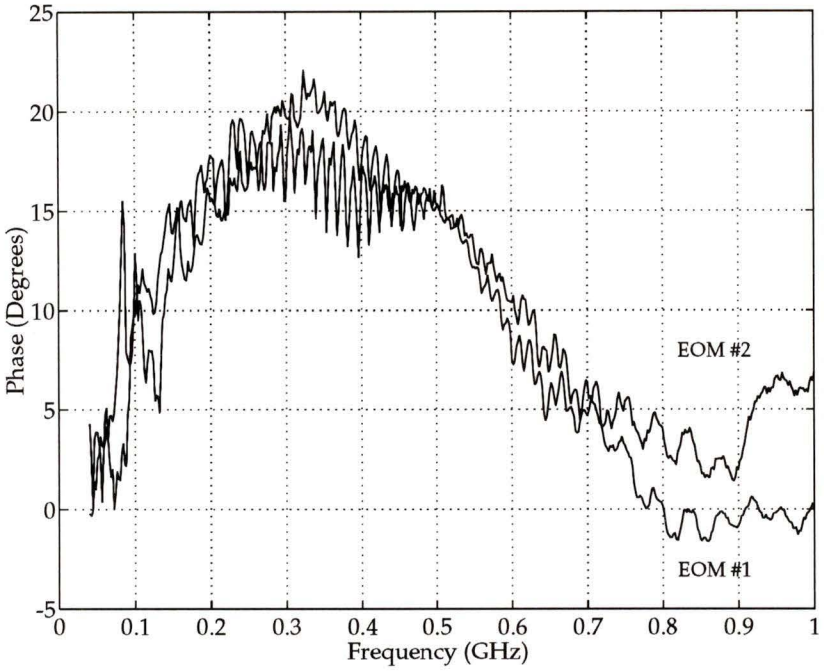

Figure 6.2 - EOM phase response

The EOM response was improved slightly by the addition of a combination bias tee and matching network placed before each EOM. This bias tee was designed to optimize the return loss looking into the modulators over the frequency range of interest. The circuit schematic for this is shown in Appendix A. The compensated transmission response for the two EOMs is shown in Figure 6.3 and Figure 6.4. It is seen from these figures that the bias tee/matching network improves the response over the frequency range of 121.25 MHz to 715.25 MHz.

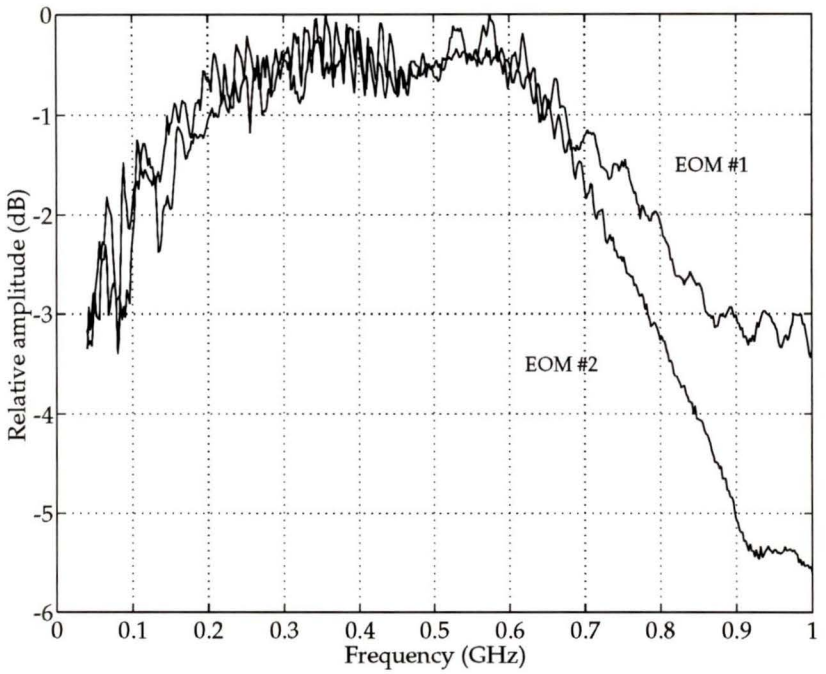

Figure 6.3 - EOM amplitude response with bias tee

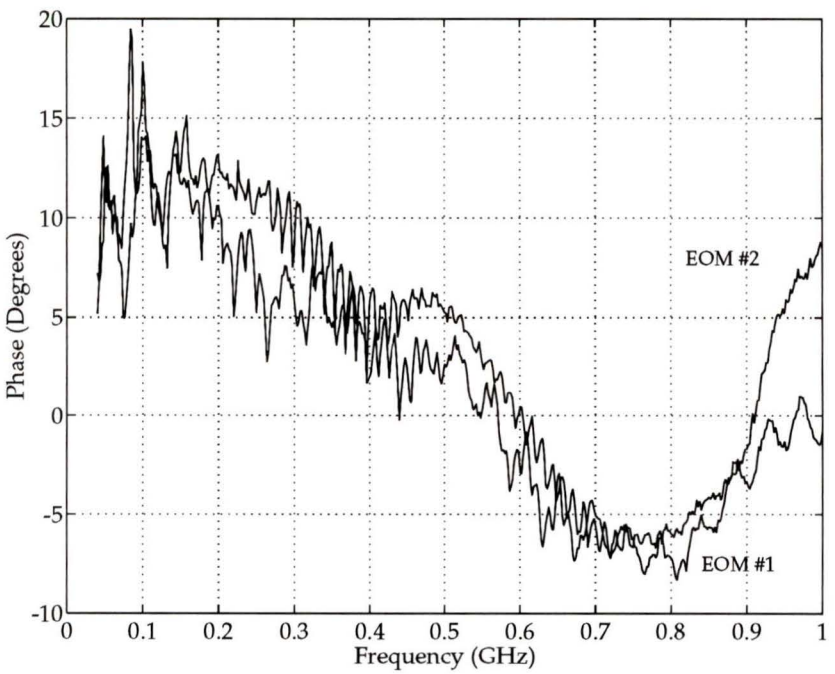

Figure 6.4 - EOM phase response with bias tee

The remainder of the amplitude and phase matching required between the electrical and optical paths is accomplished with a combination of various directional couplers, amplifiers, attenuators, phase compensators, and delays, and is the result of much tedious tuning. Directional couplers were used for amplitude matching because they exhibit a linear (in dB) rolloff of 0.7 dB between 121.25 MHz and 715.25 MHz with negligible phase distortion. The final experimental setup is shown in Figure 6.5 and 6.6, which give the optical and electrical components, respectively. A circuit schematic for the phase matching network is shown in Appendix A, and a detailed parts list of all components used in this experiment is given in Appendix B.

Figure 6.7 shows the amplitude response of the electrical and optical path at the output of the combiner. The required difference of 6 dB between the paths is obtained within ±0.5 dB. Figure 6.8 shows the phase difference between the optical and electrical paths. The required difference of 180° is obtained within ±5° up to 600 MHz; at higher frequencies the phase error increases to an unacceptable +13°.

As shown in Figure 6.6, the predistorted output signal of the combiner must be amplified so that the drive level into EOM #1 and EOM #2 is the same. The drive level into each modulator is shown in Figure 6.9. It is seen that the amplitude response to each modulator is matched to within ±0.5 dB up to 630 MHz.

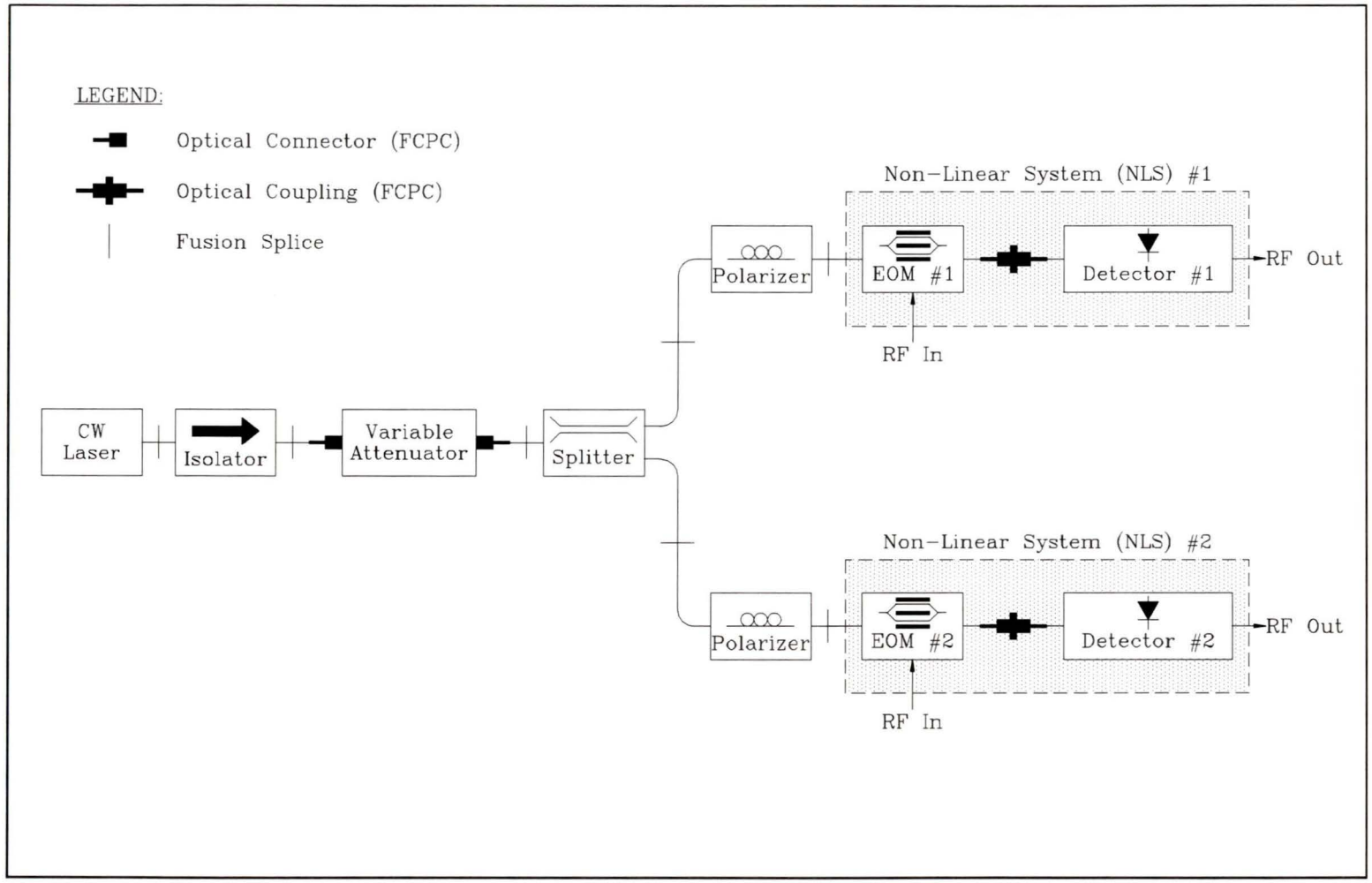

Figure 6.5 – Experimental QFF system (optical)

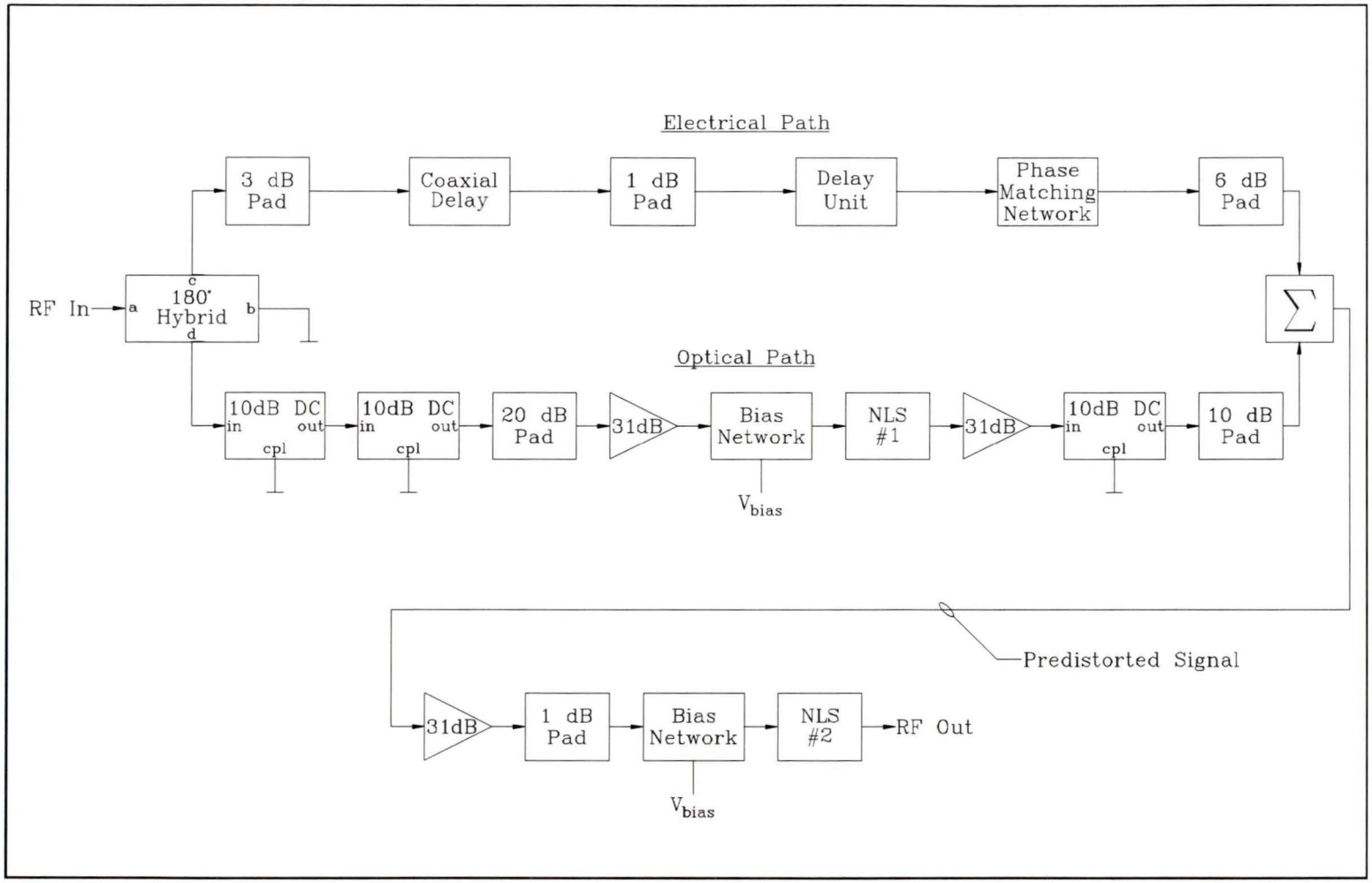

Figure 6.6 – Experimental QFF system (electrical)

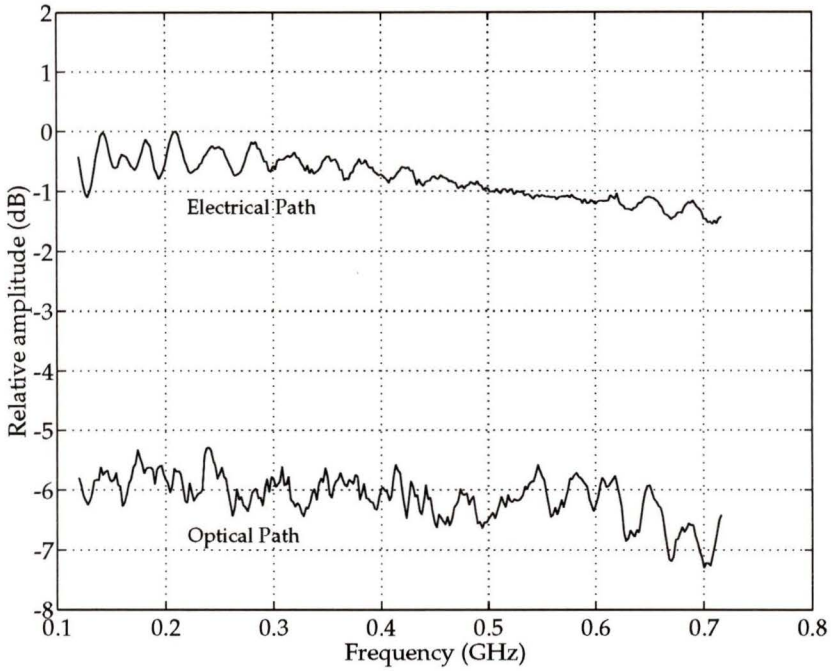

Figure 6.7 - Amplitude match at combiner

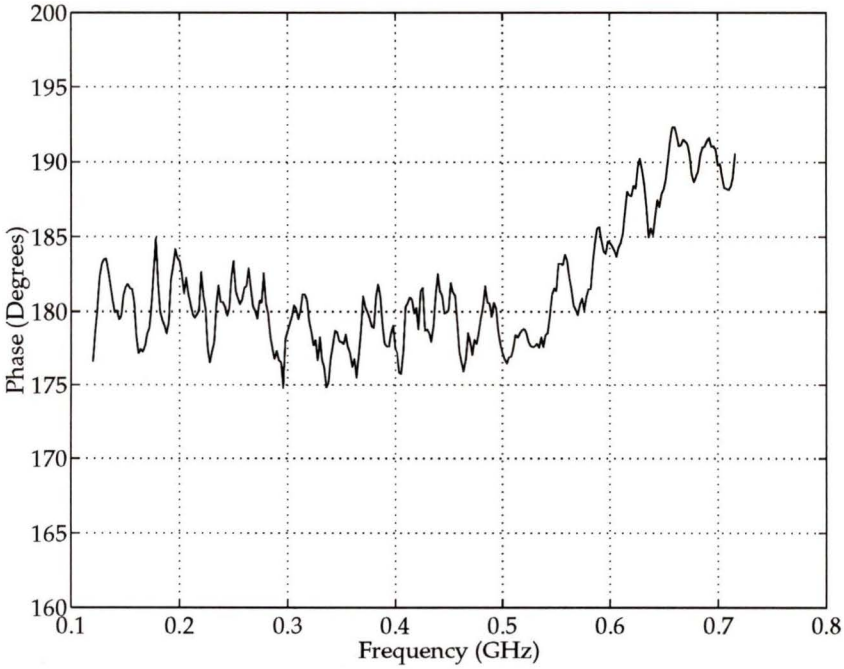

Figure 6.8 - Phase match at combiner

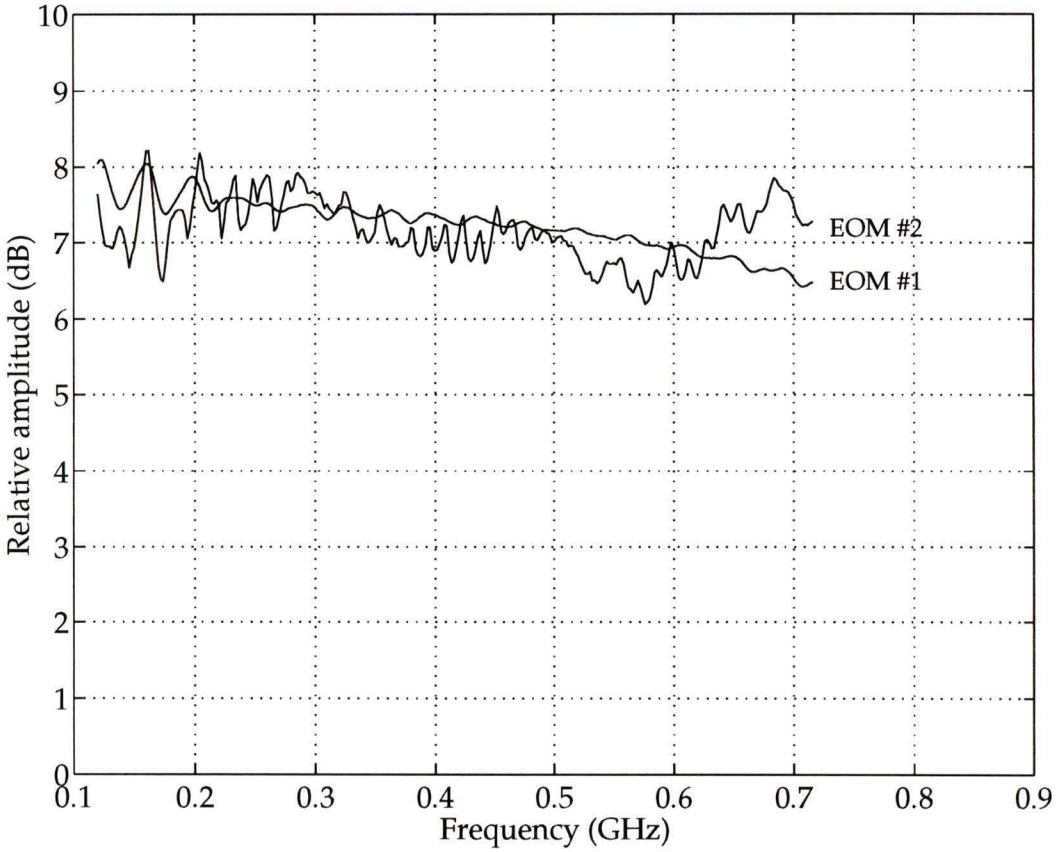

Figure 6.9 - Amplitude response from system input to bias tee of EOMs.

In summary, the performance of the experimental setup does not meet the requirements presented in Chapter 5, and hence there will be a penalty in the amount of linearity improvement obtained. The dominant source of error lies with the EOMs, which have a poor amplitude and phase reponse over the transmission bandwidth.

6.3 Two-Tone Tests

Two-tone tests were used to validate the performance of the experimental system. The test set-up is shown in Figure 6.10. An optical modulation

depth of 15% per tone was used in order to create enough distortion to be easily measured with the spectrum analyzer.

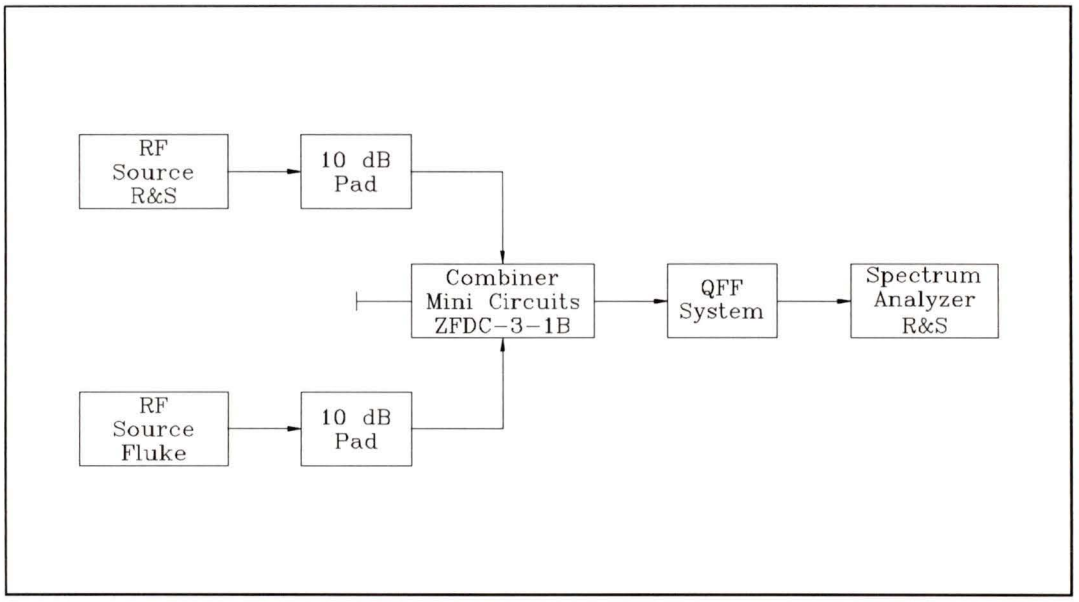

Figure 6.10 - Two-tone test setup

The measured improvement in third order IMD is shown in Table 6.1, along with the theoretical performance using the same test signals. Also shown are simulated results using measured S-parameters from the experimental system (refer to following section). It is seen from this table that an average improvement of 18 dB was achieved over the 100 channel bandwidth. The average simulated improvement using measured S-parameters was 14.6 dB. This discrepency is attributed to the poor long-term stability of the experimental setup. The distortion reduction and S-parameter measurements were performed several days apart.

Test Frequency #1 (MHz)	*Test Frequency #2 (MHz)*	*Measured Distortion Reduction (dB)*	*Theoretical Distortion Reduction (dB)*	*Simulated Distortion Reduction using Measured S-Parameters (dB)*
121.25	127.25	17.5	26.5	15.4
171.25	177.25	24.0	26.5	16.0
221.25	227.25	13.5	26.5	10.8
271.25	277.25	15.0	26.5	13.3
321.25	327.25	13.0	26.5	12.2
371.25	377.25	20.0	26.5	19.5
421.25	427.25	19.5	26.5	13.0
471.25	477.25	10.0	26.5	10.3
521.25	527.25	15.0	26.5	11.3
571.25	577.25	17.5	26.5	14.0
621.25	627.25	24.0	26.5	23.4
671.25	677.25	24.0	26.5	17.4
721.25	727.25	20.0	26.5	13.3

Table 6.1 - Two-tone test results

6.4 Simulated Predictions

Section 6.2 shows the improvement in linearity obtained with QFF using two-tone measurements. Due to the practical difficulties of generating 100 intermodulation-free test channels, the measured S-parameters from the experimental setup have been used to simulate the distortion improvement which can be achieved.

S21-parameters were measured for three paths: the electrical path from the system input to the combiner output, the optical path from the system input to the combiner output, and the optical path from the combiner output to the system output. The S-parameters were measured from 40 MHz to 750 MHz in 1.5 MHz increments, and from 750 MHz to 8.25 GHz in 15 MHz increments. These measurements were then interpolated to create 65536 points between DC and 8.25 GHz.

The simulation software was written in MATLAB. A documented listing of the program is given in Appendix C. The results of the simulation are shown in Figure 6.11 and 6.12. Figure 6.11 shows the 100 channel spectrum at the output of the first modulator, and Figure 6.12 shows it at the output of the second (linearized) modulator. The modulation depth is 1.7% per channel in both cases. This modulation depth is as high as possible without bringing distortion products above -60 dBc within the transmission bandwidth. This represents a large improvement from the 0.7% per channel possible with a single modulator. It also shows that some improvement is needed to bring the results up to the 2.2% per channel predicted in Chapter 5.

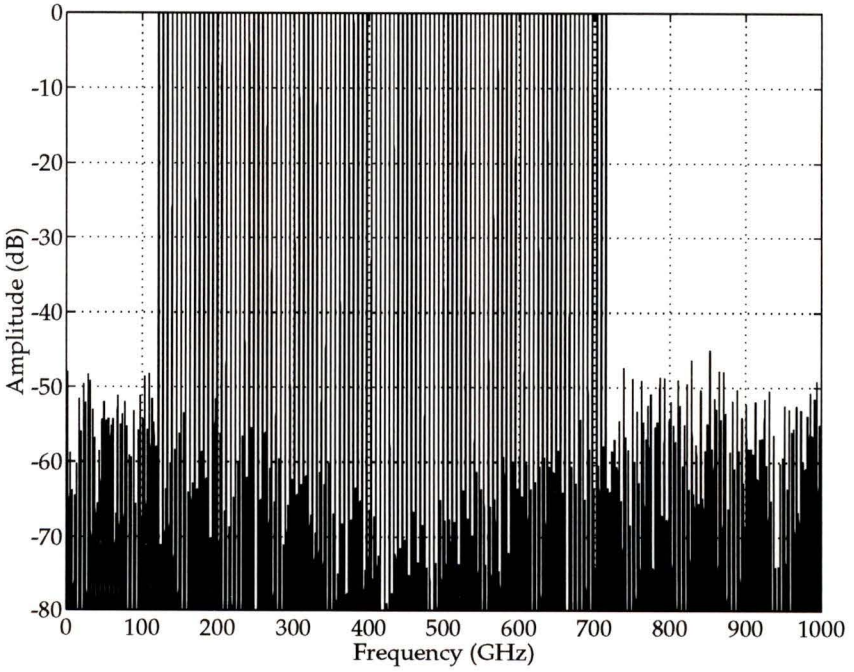

Figure 6.11 - EOM #1 output with 100 simulated input channels.

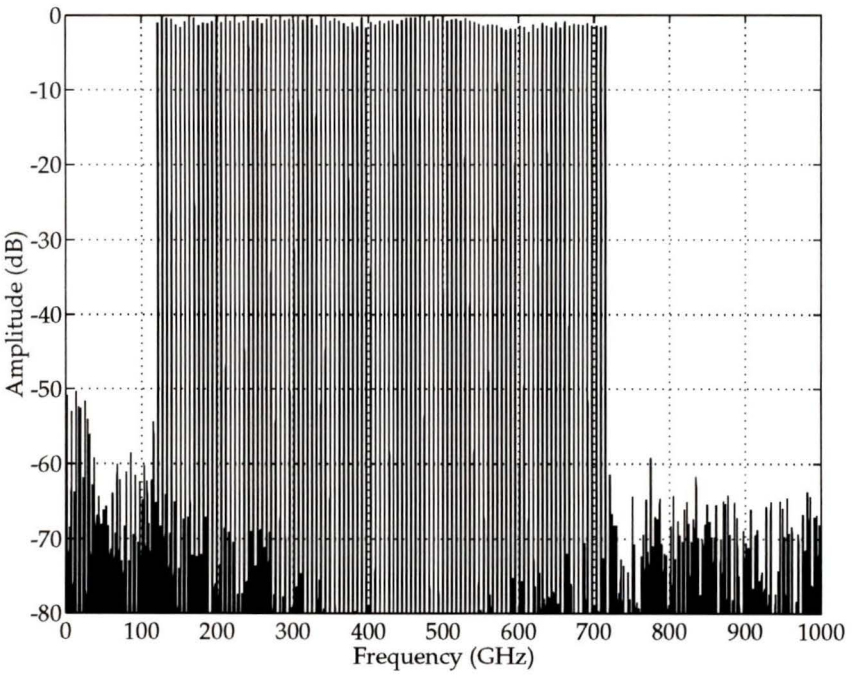

Figure 6.12 - QFF output with 100 simulated input channels.

7. CONCLUSIONS

This thesis has examined the transmission of subcarrier multiplexed AM signals over a fibre optic link, with particular emphasis on the transmission of cable television (CATV) signals. This signal format is difficult to transmit over a fibre optic link because it is very sensitive to noise and non-linear distortion.

A typical fibre optic link comprises three basic components: a transmitter (either laser diode or CW source with external modulator), some fibre, and a receiver. Of these three components, the transmitter is the dominant source of noise and non-linear distortion. Limitations due to the fibre, such as dispersion and stimulated scattering, can be overcome with careful design. The receiver does not degrade system performance as it is very linear, and the noise it produces is insignificant for the high received power levels (>0 dBm) considered in this research.

A sensitive compromise exists between noise and linearity of a laser diode. The noise cannot be eliminated but only made insignificant by increasing the per-channel modulation depth of the laser. The modulation depth has a theoretical upper bound of 4.5% per channel for a 100 channel system in order to prevent overmodulation. In reality, modulation depths of less than 1% per channel are necessary in order to keep distortion products below -60 dBc. This low modulation depth gives an unacceptable carrier-to-noise ratio.

Linearization of the optical transmitter is the only solution to this problem without increasing the received optical power to unrealistic levels. Many techniques exist for linearization including pre-distortion, feedforward, and

quasi-feedforward. These techniques are equally applicable to directly modulated laser diodes or to CW lasers with external modulators. The quasi-feedforward approach has been investigated in this thesis for use with electrooptic modulators because it offers several advantages over the other linearization schemes. These include a single optical source, no dispersion penalty, and laser RIN reduction.

The quasi-feedforward scheme is capable of transmitting 100 channels at an optical modulation depth of 2.2% per channel while satisfying the noise and linearity requirements of CATV distribution. This represents a large improvement over a conventional Mach-Zehnder modulator, which can only be modulated at 0.7% per channel. In addition, the QFF scheme gives a significant reduction in RIN for noisy optical sources, which allows the use of an inexpensive Fabry-Perot laser in place of an expensive Nd:YAG CW source.

The performance of this system was verified experimentally using discrete components. Measured distortion using two-tone tests showed an average 18 dB improvement in third order IMD over the 100 channel bandwidth. Measured S-parameters from the experimental setup were also used to simulate the performance of the system with 100 CW carriers. This simulation showed that 100 channels could be transmitted at a modulation depth of 1.7% per channel.

The experimental results could be improved significantly by using an external modulator optimized for use from DC to 1 GHz. In addition, integration of the entire system onto a single PCB would help to eliminate

many of the losses and mismatches due to the many connectors and cables used in the system.

Future work in this area should include a theoretical analysis of system performance using a noisy high-power Fabry-Perot multi-mode laser diode in place of the Nd:YAG laser. Additionally, the experimental component of this research should be further optimized and integrated in order to improve performance.

REFERENCES

[1] J. Straus and O. I. Szentesi, "Linearization of optical transmitters by a quasifeedforward compensation technique", Electron Letters, 1977, Vol. 13, No. 6, pp. 158-159.

[2] H. Skeie and V. Johnson, "Linearization of electro-optic modulators by a cascade coupling of phase modulating electrodes", *Crystal Technology, Inc.*, Private Communication.

[3] Siegfried Geckeler, *Optical Fiber Transmission Systems*, Norwood, MA : Artech House Inc., 1987.

[4] Simon Haykin, *An Introduction to Analog and Digital Communications*, New York : John Wiley & Sons Inc., 1989.

[5] Simon Haykin, *Communication Systems*, Second Edition, New York : John Wiley & Sons Inc., 1983.

[6] James N. Slater, *Cable Television Technology*, England : Ellis Horwood Limited, 1988.

[7] Department of Communications, *Technical Standards and Procedures for Broadcasting Receiving Undertakings (Cable Television)*, Broadcast Procedure BP-23, Issue 2, January 1, 1982.

[8] William B. Jones, Jr., *Introduction to Optical Fiber Communication Systems*, New York : Holt, RineHart, and Winston, Inc., 1988.

[9] Frederick V.C. Mendis and B.T. Tan, "Overmodulation in subcarrier multiplexed video FM broad-band optical networks", *IEEE Journal on Selected Areas in Communications*, Vol. 8, No. 7, pp. 1285-1289, September 1990.

[10] Paul S. Henry, "Lightwave primer", *IEEE Journal of Quantum Electronics*, Vol. QE-21, No. 12, pp. 1862-1879, December 1985.

[11] R. G. Smith, "Optical power handling capacity of low loss optical fibers as determined by stimulated Raman and Brillouin scattering", *Applied Optics*, Vol. 11, pp. 2489-2494, November 1972.

[12] Richard B. Childs and Vincent A. O'Byrne, "Multichannel AM video transmission using a high power Nd:YAG laser and linearized external modulator", *IEEE Journal on Selected Areas in Communications*, Vol. 8, No. 7, pp. 1369-1376, September 1990.

[13] Zong-Qi Lin and William S. C. Chang, "Waveguide modulators with extended linear dynamic range - a theoretical prediction", *IEEE Photonics Technology Letters*, Vol. 2, No. 12, pp. 884-886, December 1990.

[14] Zong-Qi Lin and William S. C. Chang, "Reduction of intermodulation distortion of interferometric optical modulators through incoherent mixing of optical waves", *Electronics Letters*, Vol. 26, No. 23, pp. 1980-1982, November 1990.

[15] Steven K. Korotky and Rene M. de Ridder, "Dual parallel modulation schemes for low-distortion analog optical transmission", *IEEE Journal on Selected Areas in Communications*, Vol. 8, No. 7, pp. 1377-1381, September 1990.

[16] L. M. Johnson and H. V. Roussell, "Reduction of intermodulation distortion in interferometric optical modulators", *Optics Letters*, Vol. 13, No. 10, pp. 928-930, October 1988.

[17] R. E. Patterson, J. Straus, G. Blenman, and Tad Witkowicz, "Linearization of multichannel analog optical transmitters by quasi-feedforward compensation technique", *IEEE Transactions on Communications*, Vol. COM-27, No. 3, pp. 582-588, March 1979.

[18] L. S. Fock and R. S. Tucker, "Reduction of distortion in analogue modulated semiconductor lasers by feedforward compensation", *Electronics Letters*, Vol. 27, No. 8, pp. 669-671, April 1991.

[19] L. S. Fock and R. S. Tucker, "Simultaneous reduction of intensity noise distortion in semiconductor lasters by feedforward compensation", *Electronics Letters*, Vol. 27, No. 14, pp. 1297-1299, July 1991.

[20] Frederick V. C. Mendis and B. T. Tan, "Overmodulation in subcarrier multiplexed cideo FM broad-band optical networks", *IEEE Journal on Selected Areas in Communications*, Vol. 8, No. 7, pp. 1285-1289, September 1990.

[21] Koichi Asatani, "Nonlinearity and its compensation of semiconductor laser diodes for analog intensity modulation systems", *IEEE Transactions on Communications*, Vol. COM-28, No. 2, pp. 297-300, February 1980.

[22] J. Straus, A. J. Springthorpe, and O. I. Szentesi, "Phase-shift modulation technique for the linearisation of analogue optical transmitters", *Electronics Letters*, Vol. 13, No. 5, pp. 149-151, March 1977.

[23] Yasuhiro Aoki, Kazuhito Tajima, and Ikuo Mito, "Input power limits of single-mode optical fibers due to stimulated Brillouin scattering in optical communication systems", *Journal of Lightwave Technology*, Vol. 6, No. 5, pp. 710-719, May 1988.

[24] C. Baack, G. Elze, G. Grobkobf, F. Kraus, W. Krick, and L. Kuller, "Analogue optical transmission of 26 T.V. channels", *Electronics Letters*, Vol. 15, No. 10, pp.300-301, May 1979.

[25] Helmut K. V. Lotsch, "Theory of nonlinear distortion produced in a semiconductor diode", *IEEE Transactions on Electron Devices*, Vol. ED-15, No. 5, pp. 294-307. May 1968.

[26] M. Nazarathy, C. H. Gall, S. Mukherjee, and Y. Kagan, "Predistortion linearization", *Communications Engineering and Design*, pp. 60-76, March 1992.

[27] Rod C. Alferness, "Waveguide electrooptic modulators", *IEEE Transactions on Microwave Theory and Techniques*, Vol. MTT-30, No. 8, pp. 1121-1137, August 1982.

[28] Fumio Koyama and Kenichi Iga, "Frequency chirping in external modulators", *Journal of Lightwave Technology*, Vol. 6, No. 1, pp. 87-93, January 1988.

[29] W. E. Stephens and T. R. Joseph, "System characteristics of direct modulated and externally modulated RF fiber-optic links", *Journal of Lightwave Technology*, Vol. LT-5, No. 3, pp. 380-387, March 1987.

[30] Ken-Ichi Sato, "Intensity noise of semiconductor laser diodes in fiber optic analog video transmission", *IEEE Journal of Quantum Electronics*, Vol. QE-19, No. 9, pp. 1380-1391, September 1983.

[31] Klaus Peterman and Gunther Arnold, "Noise and distortion characteristics of semiconductor lasers in optical fiber communication systems", *IEEE Journal of Quantum Electronics*, Vol. QE-18, No. 4, pp. 543-555, April 1982.

[32] Janet Lehr Jackel and John J. Johnson, "Nonsymmetric Mach-Zehnder interferometers used as low-drive-voltage modulators", *Journal of Lightwave Technology*, Vol. 6, No. 8, pp. 1348-1351, August 1988.

[33] Robert Olshansky, Vincent A. Lanzisera, and Paul M. Hill, "Subcarrier multiplexed lightwave systems for broad-band distribution", *Journal of Lightwave Technology*, Vol. 7, No. 9, pp. 1329-1342, September 1989.

[34] Winston I. Way, "Subcarrier multiplexed lightwave system design considerations for subscriber loop applications", *Journal of Lightwave Technology*, Vol. 7, No. 11, pp. 1806-1818, November 1989.

[35] David Hassin, *Laser linearization and System Considerations for AM Cable TV*, M.A.Sc. thesis, University of Victoria, 1993.

[36] Eugene Trundle, *Television and Video Engineer's Pocket Book*, London : Heinemann Professional Publishing Limited, 1987.

[37] Milton S. Kiver and Milton Kaufman, *Television Electronics*, New York : Van Nostrand Reinhold Company Inc., 1983.

[38] K. Blair Benson, *Television Engineering Handbook*, New York : McGraw-Hill Book Company, 1986.

[39] Ru van Wezel, *Video Handbook*, London : William Heinemann Limited, 1987.

[40] Joseph C. Palais, *Fiber Optic Communications*, New Jersey : Prentice Hall, 1988.

[41] Monte Ross, *Laser Receivers*, New York : John Wiley & Sons, Inc., 1966.

[42] John Senoir, *Optical Fiber Communications Principle and Practice*, London : Prentice-Hall International, Inc., 1985.

[43] Stavros Iezekiel and Christopher M. Snowden, "Nonlinear circuit analysis of laser diodes under microwave direct modulation", IEEE *MTT-S Digest*, pp. 937-940, 1990.

[44] Simon Ramo, John R. Whinnery, and Theorore Van Duzer, *Fields and Waves in Communication Electronics*, New York : John Wiley & Sons, 1984.

[45] A. R. Chraplyvy and P. S. Henry, "Performance degradation due to stimulated Raman scattering in wavelength-division-multiplexed optical-fibre systems", *Electronics Letters*, Vol. 19, No. 16, pp. 641-643, August 1983.

[46] R. W. Tkach and A. R. Chraplyvy, "Impact of fiber nonlinearities on megameter lightwave systems with optical amplifiers", *OFC Proceedings*, pp. 6, 1992.

[47] A. A. M. Saleh, "Fundamental limit on number of channels in subcarrier-multiplexed lightwave CATV systems", *Electronics Letters*, Vol. 25, No. 12, pp. 776-777, June 1989.

[48] C. P. Sandbank, *Optical Fibre Communication Systems*, New York : John Wiley & Sons, 1980.

[49] Gerd Keiser, *Optical Fibre Communications*, New York : McGraw-Hill, Inc., 1983.

[50] R. S. Roberts, *Television Engineering - Broadcast, Cable and Satellite*, London : Pentech Press, 1985.

[51] T. E. Darcie and G. E. Bodeep, "Lightwave multi-channel analog AM video distribution systems", *Proc. International Conference on Communications*, ICC '89, Houston, Texas, Paper WK2, February 1989

APPENDIX A - CIRCUIT SCHEMATICS

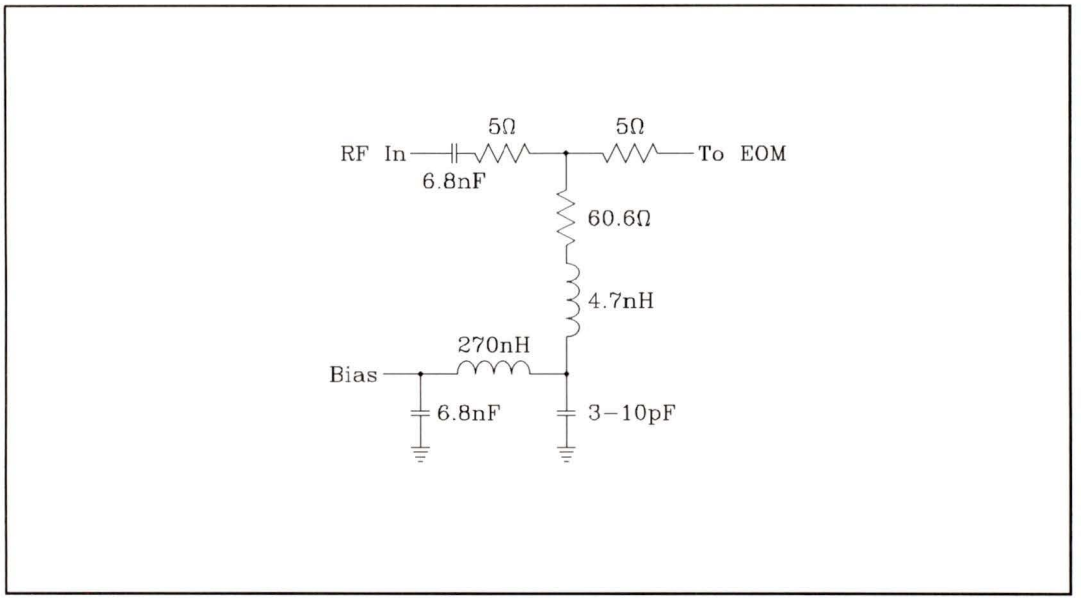

Bias Tee & Matching Network for EOM's

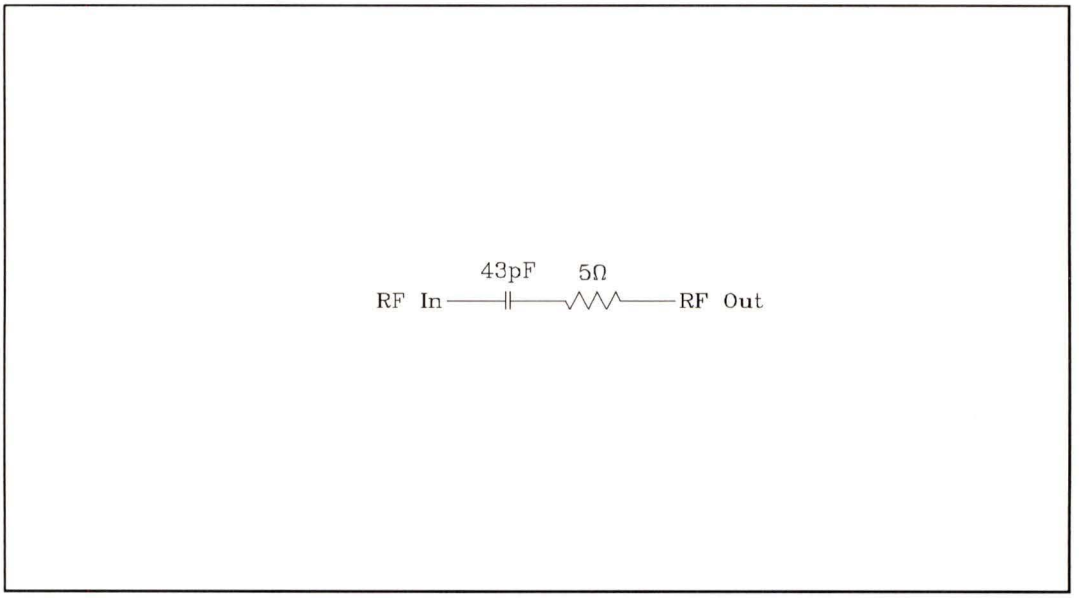

Phase Matching Network

APPENDIX B - PARTS LIST

The following tables summarize the parts and test equipment used in quasi-feedforward experiment:

Optical Components	*Manufacturer*	*Part No.*
CW Laser	Amoco Laser Company	ALC D200
Isolator	AT&T	Astrotec
Coupler	Canstar	SF3-G-1300-S
Electrooptic Modulator	GEC Marconi	Y-35-5600-01
Photodetector	Epitaxx	EPM700K

Electrical Components	*Manufacturer*	*Part No.*
Amplifiers	Mini Circuits	ZFL-1000H
Attenuators (Electrical)	Mini Circuits	SAT series
Phase Delay	Sage Laboratories	6701-23
Splitter	Mini Circuits	ZFSC-2-2500
Directional Coupler	Mini Circuits	ZFDC-10-1
180° Hybrid	Anzac	H-1-4

Test Equipment	*Manufacturer*	*Model No.*
Vector Network Analyzer	Wiltron	360B
Spectrum Analyzer	Rhode & Schartz	FSM 100 Hz - 26.5 GHz
Signal Generator	Rhode & Schartz	SMGU 100 KHz - 2160 MHz
	Fluke	6060B 10 KHz - 1050 MHz
Power Supplies	Anatek	6007/6030
Optical Attenuator	JDS Fitel	HA7503-PPU2
Optical Power Meter	3M Photodyne	2285XQ
Optical Power Meter/Receiver	Tektronix	OCP5502

APPENDIX C - SIMULATION PROGRAM

```
% ------------------------------------------------------------------
% program to simulate QFF performance using measured S21 parameters
% ------------------------------------------------------------------

rand('uniform');          % uniform phase distribution
numpts = 65536;           % number of points for FFT and IFFT
fdiv = 0.25e+6;           % frequency per division
maxch = 100;              % maximum number of channels
chspc = 6e6;              % channel spacing
ch1 = 121.25e6;           % frequency of first channel
numch = 100;              % actual number of channels
m = 0.017;                % optical modulation depth per channel
ideal = 0;                % test flag, 1 = ideal S21, 2 = measured S21

% ------------------------------------------------------------------
% load in S-parameter files
% ------------------------------------------------------------------

fprintf('\n\n\n\nLoading S-parameter files\n');

if exist('su') == 0,      % don't load if already here
   load s21a; su = s';    % electrical path from input to combiner
   load s21b; sv = s';    % optical path from input to combiner
   load s21c; sw = s';    % optical path from combiner to output
end;

% ------------------------------------------------------------------
% assign either ideal S-params or measured S-params
% ------------------------------------------------------------------

if ideal,
   sa = 2*ones(1,65536); sb = -ones(1,65536); sc = ones(1,65536);
else
   sa = su; sb = sv; sc = sw;
end;

% ------------------------------------------------------------------
% create frequency domain vector of 100 channels
% ------------------------------------------------------------------

fprintf('Creating Frequency Vector\n');
fmax = ch1 + (maxch-1)*chspc;
fs = fdiv * numpts;
f = zeros(1,numpts);

for i = 1:numch,
   if (i < 85) | (i > 88),
      fch = ch1 + (i-1)*chspc;
      ind = round(fch/fdiv);
      theta = rand*2*pi;
      f(ind) = cos(theta) + j*sin(theta);
      f(numpts-ind) = conj(f(ind));
   end;
end;
hold off;
```

```
% ------------------------------------------------------------------
% path through EOM #1
% ------------------------------------------------------------------

fprintf('First EOM\n');

% normalize amplitude of input frequencies such that a uniform
% modulation depth is obtained for each channel

f(1:65535) = f(1:65535)./abs(sb(1:65535);

% convert to time domain

fprintf('   Converting to time domain\n');
t1 = ifft(f.*sb);       % multiply by S21
vu = abs(t1)*(numpts/2);

% run through non-linear xfer characteristic of EOM #1

t1 = t1.*abs(sin(vu*m))./(vu*m);

% convert back to frequency domain

fprintf('   Converting to frequency domain\n');
f1 = fft(t1);

% plot response after EOM #1

fax = [1:1:numpts]*fdiv/1e6;
axis([fax(1) fax(4000) -80 0]);
plot(fax(1:4000),20*log10(abs(f1(1:4000))));
title('Without Linearization');
xlabel('Frequency (MHz)');
ylabel('Amplitude (dB)');
pause(1);

% ------------------------------------------------------------------
% error signal (in frequency domain)
% ------------------------------------------------------------------

f2 = 1.05*(f.*sa)+f1;

% ------------------------------------------------------------------
% path through second modulator
% ------------------------------------------------------------------

fprintf('Second EOM\n');
ftt = f2.*sc;     % multiply by S-params
fttt = ftt/max(abs(ftt(485:2861)));

% convert to time domain

fprintf('   Converting to time domain\n');
t2 = ifft(fttt*1.05);
```

```
% run through non-linear xfer characteristic of EOM #2

vu = abs(t2)*(numpts/2);
t2 = t2.*abs(sin(vu*m))./(vu*m);

% convert back to frequency domain

fprintf('   Converting to frequency domain\n');
f3 = fft(t2);

% plot results

axis([fax(1) fax(4000) -80 0]);
plot(fax(1:4000),20*log10(abs(f3(1:4000))));
title('With Linearization');
xlabel('Frequency (MHz)');
ylabel('Amplitude (dB)');
```

APPENDIX D - ABBREVIATIONS

AWGN - Additive White Gaussian Noise
CATV - Cable Television
CSO - Composite Second Order
CNR - Carrier-to-Noise Ratio
CTB - Composite Triple Beat
CW - Continuous Wave
DFB - Distributed Feedback
EOM - Electrooptic Modulator
FFT - Fast Fourier Transform
FM - Frequency Modulation
HI - Harmonic/Intermodulation
IMD - Intermodulation Distortion
IRE - Institute of Radio Engineers
LED - Light Emitting Diode
MZ - Mach-Zehnder
NTSC - National Television Standards Committee
OMD - Optical Modulation Depth
QFF - Quasi-Feedforward
RF - Radio Frequency
RIN - Relative Intensity Noise
SBS - Stimulated Brillouin Scattering
SCM - Subcarrier Multiplexed
SNR - Signal-to-Noise Ratio
SPM - Self Phase Modulation
SRS - Stimulated Raman Scattering
VSB-AM - Vestigial Sideband - Amplitude Modulated

VITA

Surname: Davidson Given Names: D'Arcy John

Place of Birth: White Rock, British Columbia, Canada

Educational Institutions Attended:

University of Victoria, Canada 1985-1995

Degrees Awarded:

B.Eng. University of Victoria, Canada 1990

Honours and Awards:

NSERC Scholarship 1991-1992
University of Victoria President's Research Scholarship 1991-1992

Publications:

1. D. Hassin, D. Davidson and R. Vahldieck, "Simulation of various linearization schemes involving external modulators and directly modulated lasers - a comparison", *Technical Papers of Canadian Cable Television Association Convention*, Vancouver, Canada, pp. 128-132, May 31 - June 3, 1992.

2. D. Davidson and R. Vahldieck, "Quasi-feedforward linearization of electrooptic modulators for analog signal transmission", *Optical Engineering*, Vol. 32, No. 4, pp. 730-734, April 1993.

PARTIAL COPYRIGHT LICENSE

I hereby grant the right to lend my thesis to users of the University of Victoria Library, and to make single copies only for such users or in response to a request from the Library of any other university, or similar institution, on its behalf or for one of its users. I further agree that permission for extensive copying of this thesis for scholarly purposes may be granted by me or a member of the University designated by me. It is understood that copying or publication of this thesis for financial gain shall not be allowed without my written permission.

Title of Thesis:

Optical Transmission Systems for Cable Television Applications

Author: 

D'Arcy John Davidson
September 29, 1995.